Biogeosciences Discuss., 10, 7299–7366, 2013
www.biogeosciences-discuss.net/10/7299/2013/
doi:10.5194/bgd-10-7299-2013

Biogeosciences Discussions
Open Access

Simulating boreal forest carbon dynamics after stand-replacing fire disturbance: insights from a global process-based vegetation model

C. Yue[1], P. Ciais[1], S. Luyssaert[1], P. Cadule[1], J. Harden[2], J. Randerson[3], V. Bellassen[4], T. Wang[1], S. L. Piao[5], B. Poulter[1], and N. Viovy[1]

[1]Laboratoire des Sciences du Climat et de l'Environnement, LSCE CEA CNRS UVSQ, UMR8212, 91191 Gif Sur Yvette, France
[2]US Geological Survey, Menlo Park, CA, USA
[3]Department of Earth System Science, University of California, Irvine, California, USA
[4]CDC Climat, 47 rue de la Victoire, 75009 Paris, France
[5]Department of Ecology, College of Urban and Environmental Science, Peking University, Beijing 100871, China

Received: 12 March 2013 – Accepted: 9 April 2013 – Published: 24 April 2013

Correspondence to: C. Yue (chao.yue@lsce.ipsl.fr)

Published by Copernicus Publications on behalf of the European Geosciences Union.

Abstract

Stand-replacing fires are the dominant fire type in North American boreal forest and leave a historical legacy of a mosaic landscape of different aged forest cohorts. To accurately quantify the role of fire in historical and current regional forest carbon balance using models, one needs to explicitly simulate the new forest cohort that is established after fire. The present study adapted the global process-based vegetation model ORCHIDEE to simulate boreal forest fire CO_2 emissions and follow-up recovery after a stand-replacing fire, with representation of postfire new cohort establishment, forest stand structure and the following self-thinning process. Simulation results are evaluated against three clusters of postfire forest chronosequence observations in Canada and Alaska. Evaluation variables for simulated postfire carbon dynamics include: fire carbon emissions, CO_2 fluxes (gross primary production, total ecosystem respiration and net ecosystem exchange), leaf area index (LAI), and biometric measurements (aboveground biomass carbon, forest floor carbon, woody debris carbon, stand individual density, stand basal area, and mean diameter at breast height). The model simulation results, when forced by local climate and the atmospheric CO_2 history on each chronosequence site, generally match the observed CO_2 fluxes and carbon stock data well, with model-measurement mean square root of deviation comparable with measurement accuracy (for CO_2 flux $\sim 100\,g\,C\,m^{-2}\,yr^{-1}$, for biomass carbon $\sim 1000\,g\,C\,m^{-2}$ and for soil carbon $\sim 2000\,g\,C\,m^{-2}$). We find that current postfire forest carbon sink on evaluation sites observed by chronosequence methods is mainly driven by historical atmospheric CO_2 increase when forests recover from fire disturbance. Historical climate generally exerts a negative effect, probably due to increasing water stress caused by significant temperature increase without sufficient increase in precipitation. Our simulation results demonstrate that a global vegetation model such as ORCHIDEE is able to capture the essential ecosystem processes in fire-disturbed boreal forests and produces satisfactory results in terms of both carbon fluxes and

BGD
10, 7299–7366, 2013

carbon stocks evolution after fire, making it suitable for regional simulations in boreal regions where fire regimes play a key role on ecosystem carbon balance.

1 Introduction

The boreal forest stores a large amount of global terrestrial ecosystem carbon, with 78 Pg C in biomass and ~230 Pg C in soil (Kasischke, 2000). This forest biome has been estimated to be a carbon sink over the late 20th century (Kurz and Apps, 1999; McGuire et al., 2009; Pan et al., 2011), but the carbon stock and carbon sink are highly sensitive to fire disturbance (Balshi et al., 2009; Bond-Lamberty et al., 2007b). Particularly, forests in boreal North America were threatened to become carbon source in the past decade due to increased fire and insect disturbances (Hayes et al., 2011; Stinson et al., 2011). Fire frequency and severity and their changes thus play a key role in controlling large-scale boreal forest carbon dynamics (Balshi et al., 2007; Bond-Lamberty et al., 2007b; Harden et al., 2000; Hayes et al., 2011).

Stand-replacing fires are the major natural disturbance in the North American boreal forest and often lead to complete forest regeneration. The time since disturbance is often an important ecosystem state variable determining the carbon flux and carbon stock (Litvak et al., 2003; Pregitzer and Euskirchen, 2004; Amiro et al., 2006, 2010). Forest age in general is recognized as a key factor in explaining the magnitude and balance of the carbon fluxes of North American boreal forests (Kurz and Apps, 1999; Kurz et al., 2009; Stinson et al., 2011). Thus this stand age effect must be included into biogeochemical models in attributing and projecting regional carbon balance.

The conceptual framework by Seiler and Crutzen (1980) used the equation $C_t = ABf_c$ to calculate fire carbon emissions, where A is the area burned, B is the biomass density or fuel load, and f_c is the fraction of biomass consumed in the burn. This method has been followed by many fire carbon emission studies with biogeochemical models for North American boreal forests (Balshi et al., 2007; French et al., 2002; van der Werf et al., 2006, 2010). Despite serving as a simple and effective approach for estimating

BGD
10, 7299–7366, 2013

emissions, the Seiler and Crutzen paradigm does not address the longer-term ecological consequence of a crown fire: trees are generally completely killed (although with a possible delay in time) leaving a large amount of snags (i.e. standing dead biomass) to be decomposed (Amiro et al., 2006; Liu et al., 2005; Manies et al., 2005), and a secondary ecosystem succession is initiated with a new forest cohort being established (Kasischke et al., 1995). The representation of stand age distributions and successional processes in biogeochemical models is an important prerequisite for accurately simulating regional carbon dynamics and interannual variability of the land-atmosphere carbon exchange.

In this study we adapted a general process-based global vegetation model ORCHIDEE (**Or**ganizing **C**arbon and **H**ydrology in **D**ynamic **E**cosystems, Krinner et al., 2005) to simulate carbon dynamics of boreal forests after stand-replacing fires, as a first step to move toward a spatially explicit cohort-based approach for regional carbon balance simulation. Three important processes are included in our model after modification. First, the fire effect is simulated in a way to generate a new forest cohort with the ground fuel and live biomass fuel being partly consumed. Second, the postfire forest regrowth is simulated with an explicit forest stand structure. Third, the fire caused snag pool and its long-term impact on ecosystem carbon balance is included.

We then calibrate and evaluate model simulations against observations from three clusters of fire chronosequence sites in North America boreal forests. The objectives of this study are:

- To perform a calibration of the model by adjusting its parameters simultaneously on CO_2 fluxes (gross primary production or GPP, net ecosystem production or NEP, total ecosystem respiration or TER), and on carbon stocks (total and aboveground biomass carbon stock, forest floor carbon stock, woody debris carbon, mineral soil carbon), and forest stand structure (basal area, stand density, mean Diameter at Breast Height or DBH).

BGD
10, 7299–7366, 2013

– To evaluate the model performance at different sites across different soil drainage conditions.

– To attribute the effects of climate and atmospheric CO_2 trends in driving the post-fire trajectory carbon fluxes at the sites examined.

– To quantify the uncertainty budget for CO_2 fluxes and the residual model biases which cannot be reduced by calibration, in order to assess the modeled carbon balance uncertainty for regional scale applications.

2 Materials and methods

2.1 Site descriptions

Three clusters of chronosequence sites distributed across the boreal forest biome in North America are used in this study (Fig. 1, Table 1). The sites include three flux towers (US-Bn1 to US-Bn3) in Alaska, seven flux towers (CA-NS1 to CA-NS7) in western Manitoba, Canada and another three flux towers (CA-SF1 to CA-SF3) in Saskatchewan, Canada (Fig. 1). The climate conditions differ among the three clusters, with mean annual temperature (MAT) as −2.1 °C for Alaska, −3.2 °C for Manitoba as and 0.4 °C for Saskatchewan, and mean annual precipitation (MAP) 290 mm for Alaska, 536 mm for Manitoba and 470 mm for Saskatchewan.

Information is available for the occurrence year of the most recent fire event on these sites. Eddy covariance (EC) methods are used to measure CO_2 fluxes for different times after fire disturbance (Table 1). For the clarity of description, the fire events listed in Table 1 are hereinafter referred to as "the most recent fire event", and the periods during which EC observations have been done are referred to as "the EC observation period". The individual EC measurement locations with multiple towers (US-Bn1–3/CA-NS1–7/CA-SF1–3) will be referred to as "evaluation site(s)".

BGD
10, 7299–7366, 2013

All the study sites are documented to have experienced stand-replacing fires, with all aboveground biomass being killed in the fire, resulting in complete forest regeneration (Amiro et al., 2006; Goulden et al., 2006; Liu and Randerson, 2008). Vegetation before burning was dominated by black spruce (*Picea mariana* (Mill.) BSP) or jack pine (*Pinus banksiana* Lamb.), and was in various stages of forest recovery when measurements were collected. Dead tree boles were found to remain erect as upright intact at ~5 yr after fire, and most of these snags fell within 10–15 yr after burning (Goulden et al., 2006; Liu and Randerson, 2008). Soils at the three evaluation site clusters are moderately well drained to well drained (Gower et al., 1997; Liu et al., 2005; Goulden et al., 2006). Discontinuous permafrost layer were observed at the Alaska and Manitoba sites whereas absent in the top 2 m soil for all the Saskatchewan sites (Gower et al., 1997).

For the purpose of model evaluation, various measurements for all the evaluation variables are collected from a range of openly published studies, or retrieved by authors (Table 2). Note that not all the measurements used for our evaluation purpose were done exactly in the footprint of the flux tower, but at locations either very close to the flux tower sites, or considered as being representative of the typical boreal forest ecosystems at the evaluation sites.

2.2 Model description of ORCHIDEE_FM

ORCHIDEE_FM refers to the biogeochemical model ORCHIDEE with the novel forest management (FM) module. The ORCHIDEE Dynamic Global Vegetation Model (DGVM) designed for largescale modeling applications consists of three sub-models (Krinner et al., 2005). The first sub-model SECHIBA simulates energy and water exchange between the top of canopy and the atmosphere. The second sub-model STOMATE simulates vegetation carbon processes such as photosynthesis, photosynthates allocation, plant mortality and organic matter decomposition. The third sub-model (which was built around the equations of the LPJ DGVM, see Sitch et al., 2003) simulates vegetation dynamics. For the current study, only the first two sub-models are used and the dynamic vegetation sub-model is switched off.

BGD
10, 7299–7366, 2013

Brought to steady equilibrium state for vegetation and soil carbon pools after a long spin-up, ORCHIDEE originally represents an "average" mature forest in a big-leaf approximation. To explicitly account for forest stand structure and forest age, a forest management module (FM) was developed (Bellassen et al., 2010) for better representation of forest development. The version of ORCHDEE with FM module is hereinafter referred to as "ORCHIDEE_FM", and the original ORCHDEE (without FM) will be referred to as "the standard version of ORCHIDEE".

ORCHIDEE_FM included several processes that are important to simulate forest stand development: (1) age-related stand dynamic processes are modeled, including the decline in NPP in old forests, and age limitation of leaf area index (LAI) growth in young stands, and age-dependent allocation of woody NPP among stem and coarse root. (2) A woody litter pool is added to account for the slow decomposition of tree woody litter. (3) Branch mortality is explicitly simulated. (4) Forest stand structure (stand density, tree diameter distribution etc.) is explicitly described and the model is able to simulate the self-thinning process, given a maximum density-biomass relationship for different types of forests.

The decomposition for above- and belowground litter and soil organic carbon is modeled to follow first order kinetic equation in ORCHIDEE_FM (Parton et al., 1988). Litter pool is divided into three types according to their residence time (at temperature of 30 °C): metabolic litter (default residence time = 0.066 yr), structural litter (default residence time = 0.245 yr), and woody litter (default residence time = 0.75 yr). When being simulated, actual litter decomposition rate depends on its residence time, litter moisture and temperature as well as the lignin content. As litter moisture and temperature are dynamically calculated by the SECHIBA sub-model, the litter decomposition rate varies with climate and time. To give an example, the mass weighted mean litter turnover time is ~ 15.7 yr for Manitoba sites when the model is driven by local climate.

Mineral soil carbon is also divided into three different pools according to their residence time (at temperature of 30 °C): the active pool (default residence time 0.149 yr), the slow pool (default residence time 5.48 yr) and the passive pool (default residence

BGD
10, 7299–7366, 2013

time 241 yr). Again, actual soil carbon decomposition rate depends on soil moisture and temperature. As an example, the mass-weighted mean soil carbon turnover time is 1555 yr at the Manitoba sites when the model is driven by local climate.

Plant live biomass is divided into 8 compartments: leaf, above- and belowground sapwood, above- and belowground heartwood, root, fruit, and carbon reserve pool. In ORCHIDEE, when the transfer of carbon from live biomass to litter happens, the carbon in live biomass does not go directly to the three litter pools, but all the live biomass goes to a temporary litter buffer, and that litter buffer is allocated to the three litter pools according to prescribed ratios (Krinner et al., 2005).

2.3 Modifications of ORCHIDEE_FM into ORCHIDEE_FM_BF for boreal fires

This section describes how ORCHIDEE_FM is adapted into ORCHIDEE_FM_BF (ORCHIDEE_FM for boreal fires) to make it able to simulate boreal crown fire processes. A crown fire kills all the aboveground biomass and initiates a new forest cohort, and is similar to a clearcut event from a successional modeling perspective, although the aboveground carbon is exported in case of clearcut. The "clearcut" routine of the FM module is thus adapted to mimic fire burning effects and the establishment of the new forest after fire. When crown fire occurs, part of the ground litter and tree biomass are removed from existing pools as carbon emissions into the atmosphere, and the unburned biomass are simulated as standing dead wood (snags), which gradually transfers to the litter pool over time.

2.3.1 Age-related changes of LAI and productivity

Previous studies have reported that LAI increases with stand age in young boreal forests until ~25 yr, and after that LAI tends to saturate (Wang et al., 2003; Goulden et al., 2011). This age dependence of LAI is empirically modeled by scaling the maximum LAI (a parameter specified for each biome in ORCHIDEE which sets an achievable climax LAI, not necessarily reached at a given site) to increase with the square

BGD
10, 7299–7366, 2013

root of stand age until 25 yr. The model's default maximum LAI of 4.5 $m^2 m^{-2}$ for the boreal forest biome is used.

To account for the productivity decrease in aging boreal forests (Bond-Lamberty et al., 2004; Mack et al., 2008; Goulden et al., 2011), a decrease in the optimal carboxylation rate in old-growth forest is added in the model's equations. For stands aged between 100 and 200 yr old, the optimal carboxylation rate is modeled to decrease by up to 10 % over the 100 yr in a linear way, to mimic the NPP reduction between a 74 yr and a 154 yr old forest in central Canada observed by Goulden et al. (2011). To make the simulated productivity in agreement with observation, the optimal carbonxylation rate is adjusted from the default value of 35 µmol $m^{-2} s^{-1}$ to 24 µmol $m^{-2} s^{-1}$.

2.3.2 Fire combustion fraction for different carbon pools

This section describes how fuel combustion fractions are determined in ORCHIDEE_FM_BF to match the observations in boreal forests. Two types of fuels are available for burning in a typical boreal forest crown fire: ground fuels, which may contain moss layer, herbs, fine litter and small shrubs; and crown fuels, which are mainly forest live biomass and shrubs if present. Regional datasets and experimental fire studies show that fire carbon emissions are dominated by ground fuels (Stocks, 1987, 1989; Amiro et al., 2001; Kasischke and Hoy, 2012). Therefore, most of the fire emissions must be modeled to come from ground fuel burning.

Previous studies indicate that fuel combustion fractions in fires are not constant and depend on multiple factors including preburn fuel load, fire weather, topographic feature of burned site, and the season of burning (De Groot et al., 2009; Turetsky et al., 2011). However the present study does not seek accurate simulation of combustion fraction and thus simple fixed combustion fractions are adopted for different types of fuel. Kasischke et al. (2000) reported a combustion fraction of 0.43 (ranging from 0.20 to 0.89) for ground fuels and 0.36 (ranging from 0.22 to 0.48) for live biomass in interior Alaskan black spruce fires. We thus assume metabolic, structural and woody litters are

BGD
10, 7299–7366, 2013

consumed by 1.0, 0.9 and 0.3, respectively during fire, which corresponds to a mass weighted mean combustion fraction of 0.3 for total ground fuel.

In boreal forest fires, the crown fuel combustion was found to be limited to small branches and needles (Stocks, 1987, 1989; Amiro et al., 2001; Kasischke and Hoy, 2012). In ORCHIDEE_FM_BF, leaf biomass is represented but branches are not accounted for explicitly. Rather, we assume that 90 % of the aboveground sapwood and 2 % of the heartwood could be considered as small branches and will be combusted in fire. These fractions are determined with the relative size of each pool being taken into account.

For aboveground biomass combustion, we set the combustion fractions for leaf, aboveground sapwood and heartwood, fruit and carbon reserve as 0.9, 0.9, 0.02, 0.7, and 0.7, respectively. Since there is no tree survival during the fire, the unburned aboveground heartwood is transferred to the snag pool, and all other unburned biomass parts (with a relatively small size) enter litter pool (via the litter buffer) immediately after fire. During fires, black carbon could be generated from incomplete burning and accumulates in the underlying mineral soil (Kane et al., 2007), but with rather a small amount and is not explicitly considered in this study.

The parameterization of fire combustion fraction and the fraction of carbon being transferred to litter for various carbon pools are summarized in Fig. 2. Under this scheme, the mass weighted mean combustion fraction is 7 % for aboveground live biomass and 30 % for ground litter.

2.3.3 Snag decay after a fire event

At the three study sites, fire formed snags and downed dead wood represent a significant component of the forest carbon stocks. In reality, the decrease of snags (either standing or downed) occurs through three processes: decomposition by microbes, fragmentation and leaching. Field measurements show that the change of snag and woody debris as a function of time after fire follows a first order kinetic equation

BGD
10, 7299–7366, 2013

(Bond-Lamberty and Gower, 2008):

$$\frac{dD}{dt} = -kD \quad (1)$$

where $\frac{dD}{dt}$ is the change of woody debris, D is the existing woody debris and k is the annual decomposition constant. Bond-Lamberty and Gower (2008) reported k value of 0.05–0.07 yr^{-1} for standing snag and downed woody debris using three independent methods: direct respiration measurement, field repeated surveys and chronoseqence observation.

To represent this process, a snag pool is added in ORCHIDEE_FM_BF, which includes the above-ground unburned heartwood biomass and belowground thick pivotal woody roots. To simplify the model, it is assumed that no respiration occurs for standing snags and that the reduced snag mass enters the litter pool completely. This is consistent with Manies et al. (2005), who found standing snags (stems) respire very slowly until they fall and come in contact with moss and soil.

During the first 20 yr after fire, we assume an annual decay rate of 8 % (k = 0.08 yr^{-1}) of snag being transferred to litter pool, and during the next 20–40 yr an annual rate of 5 % (k = 0.05 yr^{-1}). At the time of 40 yr after fire, all the remaining snags become litter. These parameters are determined after the field measurements by Bond-Lamberty and Gower (2008).

2.3.4 Modifying litter and soil carbon turnover time

The default values of litter and soil carbon turnover time in ORCHIDEE were originally defined from the CENTURY soil carbon decomposition model (Parton et al., 1988) which was based on grassland ecosystems. We modify the residence time parameters in ORCHIDEE_FM_BF according to observations of radiocarbon content (Trumbore and Harden, 1997) and mass balance constraint studies (Harden et al., 2000; O'donnell et al., 2011) for boreal soils. Practically, the respective residence times for the three aboveground litter pools (see Sect. 2.2) are increased by a factor of 3, and

BGD
10, 7299–7366, 2013

the respective residence times for the three mineral soil carbon pools are increased by 0.4 times. So when driven by local climate, the modified mass weighted mean turnover time is ∼63 yr for aboveground litter (against 15.7 yr in the standard version of ORCHIDEE) and ∼2100 yr (against 1555 yr) for mineral soil carbon pool.

2.4 Simulation set-up

2.4.1 Climate forcing data

ORCHIDEE_FM_BF is driven by high frequency (30 min resolution) but can also accommodate low frequency climate forcing data (e.g. monthly resolution). In the case of low frequency data, the model uses a weather generator to generate the 30 min climatic fields for the model input. In this study, two different sets of climate forcing data are used to drive the model.

First, monthly meteorological fields were retrieved from meteorological stations located close to the evaluation sites. For the Alaska sites, data from meteorological stations of Delta Junction (1941–2006) and Fairbanks (1930–2006) were used. For Saskatchewan sites, data from meteorological station of Prince Albert (1943–2006) were used. For Manitoba sites, data from the meteorological station of Thompson (1968–2006) were used.

For monthly climate data, 7 meteorological fields (precipitation, number of precipitation days, 2 m air relative humidity, 2 m air temperature, 2 m air temperature amplitude, total cloud cover, 10 m windspeed) were required to drive the model. Monthly temperature, monthly total precipitation and monthly temperature amplitude were available for Saskatchewan and Manitoba sites, and only monthly temperature and monthly precipitation data were available for Alaska sites. Thus for other meteorological fields that are required by the model, monthly values were extracted from the CRU3.1 data (Climate Research Unit, University of East Anglia, http://badc.nerc.ac.uk/view/badc.nerc.ac.uk__ATOM__dataent_1256223773328276) at the grid cell corresponding to the

BGD
10, 7299–7366, 2013

geolocation of each evaluation site. These monthly data are referred to as the composite monthly climate data or CMCD for brevity.

Second, in-situ meteorological measurements (with 30 min resolution) from the eddy covariance sites are used. For Manitoba and Saskatchewan sties, data are retrieved from the La Thuile dataset (http://www.fluxdata.org). Data for Alaska sites are provided by J. T. Randerson. These data were gap-filled by using the corrected daily data from ECMWF ERA-Interim (IERA) 0.7 × 0.7 degree reanalysis (for details, see Wang et al., 2012). These high frequency data are used to drive the model for only the EC observation period. Hereinafter we refer to this data as half-hourly climate data or HHCD for brevity.

2.4.2 Vegetation, soil and other input data

ORCHIDEE_FM_BF is built on the concept of plant functional type (PFT) to describe different vegetation types, with each PFT being associated to a specific vector of model parameters. Boreal evergreen needleleaf forests (black spruce or jack pine) are the climax vegetation type on the evaluation sites, although broadleaf trees such as trembling aspen often take a dominant role in the early succession stage. ORCHIDEE_FM could be prescribed to allow co-existing of different vegetation types in the same grid cell. However in our study, to simulate an even-aged cohort of boreal trees after a crown fire, each site is prescribed to be fully covered by the *boreal needleleaf evergreen forest* PFT (see Krinner et al., 2005). The PFT-specific parameters in ORCHIDEE_FM_BF are set to the model default values given by Krinner et al. (2005) except the modifications described in Sect. 2.3. Soil texture is prescribed at each site as shown in Table 1.

2.4.3 Simulation protocol

Our simulations are conducted in a way that does not require specific biometric measurement inputs (such as LAI, initial biomass, mineral soil carbon etc.). Rather, these variables are determined from climate forcing data and the model equations in a

BGD
10, 7299–7366, 2013

prognostic way, by starting with a spinup simulation and followed with transient simulations. Boreal forests are known to experience recurrent fire disturbances in history, and similarly, our simulation protocol is designed to allow a gradual ecosystem carbon pool accumulation under recurrent fires until equilibrium state, before the most recent fire event is simulated at each site (Fig. 3).

As we do not know the exact history of fire disturbances for each evaluation site, the Fire Return Interval (FRI) for all the sites is set uniformly as 160 yr. This value is chosen for three considerations. First, the oldest stand in the evaluation sites is 155 yr after fire (CA-NS1 in Manitoba). Second, the FRI for Canadian central boreal forest was reported to range between 66 and 200 years by Stocks et al. (2002). Third, Anderson et al. (2006) reported that during the past 4600 years, the FRI for a lowland boreal forest in south Alaska was 142 ± 70 yr. We acknowledge that the uniform FRI of 160 yr is a simplified assumption, as fire occurrence depends on several factors including climate (which varied during the Holocene) and the availability of fuel, and thus did not necessarily occurred at equal intervals in the past, preceding the observation period.

According to the defined simulation protocol (Fig. 3), the model is first run for an "first spinup" period starting from bare soil and without fires for 400 years, followed by a "second spinup" of 3200 yr, i.e. 20 successive "fire rotations" with assumed stand-replacing fires occurring every 160 yr (each 160 yr period is called a "fire rotation"). This second spinup allows that all forest ecosystem carbon pools (especially the mineral soil carbon pool) reach a long term equilibrium state in presence of recurrent fire disturbance. Finally, the most recent fire event is simulated for the year of burning, and the model is driven with actual climate forcing data during the postfire period of forest regrowth, so that the model output can be compared to and evaluated against field measurements.

We define a "climate forcing history" which is used by most of the simulations. The monthly CMCD climate data are used in this climate forcing history. The rationale of the climate forcing history is to ensure that, for the historical spinup, the average state of historical climate is used, and for the period before and after the most recent fire

BGD
10, 7299–7366, 2013

event, actual observed climate data is used. More specifically, the climate forcing data used in different stages of the simulation protocol are as below (see also Table 3):

1. For the first spinup and the first 19 fire rotations of the second spinup, we use the multi-year mean CMCD climate data of each site from the beginning year of meteorological station measurement until the year of most recent fire (see Table 3 for details). This stable climate forcing is used with the goal to drive the model into equilibrium state with the average state of historical climate conditions.

2. For the last (20th) fire rotation of the second spinup, at the beginning the average CMCD are used, but when entering the period of meteorological station measurement, the climate forcing shifts to actual year data. The time of shift depends on the year of most recent fire and the duration of meteorological station observation at each site. By doing so, we make sure that before the most recent fire, actual monthly climate data are used to reflect historical climate trends and variability that the ecosystem experienced at each site (see Table 3 for details).

3. For the postfire simulation after the most recent fire event, actual CMCD climate data continue to be used. But if the most recent fire occurred earlier than the start year of the meteorological station measurement, the average CMCD data are repeated until the year when meteorological station observation started and then real CMCD data begin to be used.

Two scenarios of CO_2 concentration are used in the simulations, namely fixed CO_2 (CO_2FIX) and variable CO_2 (CO_2VAR), respectively. In the CO_2FIX scenario, the atmospheric CO_2 concentration is fixed constantly at the 1850 level (285 ppm) throughout the simulation. In CO_2VAR scenario, for the "first spinup" until the 20th fire rotation of the second spinup, CO_2 concentration is fixed at the 1850 level, then during the 20th fire rotation, beginning from some point the atmospheric CO_2 is prescribed to increase (transient CO_2 concentration is used), and corresponds exactly to the CO_2 concentration at the year of burning for the most recent fire at each site. This is done to reflect

BGD
10, 7299–7366, 2013

the atmospheric CO_2history experienced at each different site. The difference between CO_2VAR and CO_2FIX allows us to separate the effect of CO_2 fertilization on postfire CO_2 fluxes.

2.4.4 List of simulations in this study

Based on the defined simulation protocol, several simulations have been done, which are listed in Table 4 and described as below:

CNT-CMCD. Control simulation. The simulation has been done using ORCHIDEE_FM_BF with all the modified features, processes, and parameters described in Sect. 2.3. The CO_2VAR scenario is used.

GPPCAL-CMCD. GPP calibration simulation. This simulation uses the same forcing with CNT-CMCD simulation, but the eddy-covariance observed multi-year mean GPP is assimilated (nudged) into the model. GPP assimilation is done by first calculating the ratio of average simulated to observed GPP at each study site for EC observation period, and then apply this site-specific ratio throughout all the simulation stages (first spinup, second spinup and postfire simulation, see Fig. 3) to correct the simulated GPP for each run step. In this manner, the mean modeled GPP is tuned to be equal with the multi-year mean value observed by eddy-covariance.

CNT-HHCD and GPPCAL-HHCD. These simulations are the same as CNT-CMCD and GPPCAL-CMCD, except that HHCD (half-hourly climate data) rather than CMCD are used during the EC observation period. Note that GPPCAL-CMCD and GPPCAL-HHCD simulations will have exactly the same GPP in every time step of the simulation (30 min) and the change of CMCD data to HHCD for EC observation period will only affect respiration, and thus net ecosystem production.

CO_2*FIX-CLIMVAR*. No CO_2 fertilization simulation. The CO_2FIX scenario was used in the simulation, with varying climate data.

CO_2*FIX-CLIMFIX*. No CO_2 fertilization simulation. The CO_2FIX scenario is used in the simulation. But for the postfire simulation after the most recent fire, input climate forcing is fixed as the average monthly climate data that is used in the spinup runs.

BGD
10, 7299–7366, 2013

This simulation together with CO_2FIX-CLIMVAR simulation are done only for sites CA-NS1, CA-SF1 and US-Bn1, in order to be compared with GPPCAL-CMCD simulation to attribute the role of varying climate and CO_2 in post-fire carbon flux trajectory. To make the results comparable with the GPPCAL-CMCD simulation, the same site-specific GPP correction ratio used in GPPCAL-CMCD simulation is applied to correct modeled GPP in each step of the CO_2FIX run.

ORC-STD. Simulation with standard version of ORCHIDEE. This simulation is done using standard version of ORCHIDEE, with the same crown fire process as in Sect. 2.3 being implemented. No snag pool is represented and all unburned live biomass is sent to the litter pool (via litter buffer) immediately after fire.

ORC-FM-NOSNAG. Simulation with ORCHIDEE_FM with the same crown fire process implemented. Again, no fire caused snag process is represented in the model. This simulation and ORC-STD simulation are mainly for comparing with CNT-CMCD simulation to demonstrate the "improvement chain" in simulating postfire forest regrowth by moving from standard ORCHIDEE to ORCHIDEE_FM and further to ORCHIDEE_FM_BF.

2.5 Method for simulation-measurement comparison

2.5.1 Match model outputs with field measurements for woody debris, forest floor and mineral soil carbon

Due to the difference in the scope of the forest floor and woody debris between field measurement and modeling, in this section we develop a scheme to match the model output with field measurement for these variables.

The terminology, measurement scope and reporting of forest woody detritus in the field are not consistent among different researchers. For example, Bond-Lamberty and Gower (2008) reported total woody detritus as the sum of standing dead wood (SDW, dead wood with zenith angle ≤ 45) and downed dead wood (DWD, woody detritus with diameter > 1 cm with zenith angle > 45). Whereas Wang et al. (2003) reported them

BGD
10, 7299–7366, 2013

as standing dead tree (STD) and coarse woody debris (CWD). Goulden et al. (2011) reported coarse woody debris, which includes downed woody debris with diameters ≥ 7 cm (Manies et al., 2005; Goulden et al., 2011). In this study, we adopt the term used by Bond-Lamberty and Gower (2008). Total woody debris (TWD) consists of standing dead wood (STD, with zenith angle ≤ 45 in field measurement), and downed woody debris (DWD, snags with zenith angle > 45 and woody detritus lying on the ground). Furthermore, in field measurement the heavily decomposed fine woody debris is always sampled as part of the forest floor or organic soil (Wang et al., 2003; Goulden et al., 2011). Thus, for the aboveground part, the sum of aboveground litter and snags in the model should be equal to the sum of forest floor and total woody debris in field measurement (Fig. 4.) As shown in Fig. 4, to compare model downed woody debris with measurement, 30 % of the aboveground snag in the model was treated as DWD. This fraction is determined in a way to make the ratio of DWD to total woody debris equal to the chronosequence average ratio reported by Bond-Lamberty and Gower (2008). The remaining 70 % of modeled snag carbon is compared with the standing dead wood in the field measurement.

To compare the modeled forest floor carbon with measurement, 75 % of aboveground woody litter in the model was counted as forest floor (Fig. 4). This fraction was selected in a way to optimize the model-measurement comparison for forest floor carbon and downed woody debris simultaneously. The remaining 25 % of modeled woody litter is counted as DWD.

Finally, the mineral soil carbon in the model is added together with belowground litter to be compared with measured mineral soil carbon. The model-data matching is summarized in Fig. 4, which allows closure of all carbon stock compartments between model and measurement.

2.5.2 Model-measurement agreement metrics

To quantitatively evaluate the simulation-measurement agreement, three metrics are used in this study:

BGD
10, 7299–7366, 2013

(1) Metrics 1. Linear regression is used to examine the overall model-measurement agreement. Simulation data are regressed against measurements with the regression line forced to pass through origin (Regression Through Origin, RTO) as it is assumed when the measurement value is zero, the simulation value should be zero as well. The RTO model used is:

$$Y_i = \text{slope} \cdot X_i + \varepsilon_i \tag{2}$$

where X_i is measurement data, Y_i is simulation data, ε_i is random error. If the regression slope is not significantly different from 1, then we consider it as fairly good agreement.

(2) Metrics 2. The Root Mean Square Deviation (RMSD) is used to quantify the model-measurement agreement in an absolute term. RMSD is the average quadratic distance between simulation and measurement values:

$$\text{RMSD} = \sqrt{\frac{\sum_i (X_i - Y_i)^2}{n}} \tag{3}$$

where Y_i and X_i are simulated and measured data, respectively. We further calculate the systematic RMSD (RMSD_sys), which describes the error caused by systematic difference between simulation and measurement data, and unbiased RMSD (RMSD_unbias), which describes the error caused by internal variation among simulation values:

$$\text{RMSD\_sys} = \sqrt{\frac{\sum_i (X_i - \hat{Y}_i)^2}{n}} \tag{4}$$

BGD
10, 7299–7366, 2013

where $\hat{Y}_i$ is the predicted value by RTO regression, X_i is measurement value.

$$\text{RMSD\_unbias} = \sqrt{\frac{\sum_i (Y_i - \hat{Y}_i)^2}{n}} \quad (5)$$

where $\hat{Y}_i$ is the predicted value by RTO regression, and Y_i is simulation value. If RMSD is close to the field measurement error (instrument error, aggregation error, site-to-site and year-to-year precision) and RMSD is dominated by RMSD_unbias, then we consider the modeling error is acceptable, and that the model realistically reproduces measurement data.

(3) Metrics 3. Measurement-simulation uncertainty overlapping ratio is used to characterize measurement-simulation agreement with uncertainties in both being considered. First, we collect for each evaluation variable the measurement standard error or 90 % confidence interval when they are reported in the source literature and treat them as the measurement uncertainty. Then we calculate the number of data points where the simulation uncertainty and the measurement uncertainty overlaps. Finally we calculate the ratio of this overlapped number to the total number of measurement data points (Bond-Lamberty et al., 2006). We consider one overlapping between model and measurement uncertainty to indicate that the model is able to simulate correctly the measurement. When doing above, model simulation uncertainty is constructed by pooling together simulation data for all the evaluation sites at the same site cluster, and the minimum-maximum range among model output is treated as simulation uncertainty.

As soil drainage condition is recognized as an important site-specific feature affecting forest ecosystem processes in North American boreal forests (Wang et al., 2003; Yi et al., 2009), and therefore model-data misfit, all the measurement data have been classified as either “dry” (with good soil drainage) or “wet” (with poor soil drainage) according to the information provided in data source literature. As noted in Sect. 2.1,

BGD
10, 7299–7366, 2013

all the evaluation sites simulated could be considered as dry sites. Nevertheless, to have an idea on the model performance for the poor-drainage sites as well, the model-measurement comparison statistics by metrics (1), (2), and (3) are calculated separately for "dry" and "wet" sites, and for all dry and wet sites combined.

3 Results

3.1 Model improvement in ORCHIDEE_FM_BF compared to the standard verison

Figure 5 shows the simulated GPP, NEP, heterotrophic respiration and total biomass carbon for the 19th, 20th fire rotation and the postfire simulation by ORC-STD, ORC-FM-NOSNAG and GPPCAL-CMCD simulations, for the sites in Manitoba.

Moving from standard ORCHIDEE to ORCHIDEE_FM (or ORCHIDEE_FM_BF) significantly improved simulation results. Simulated GPP, total biomass carbon and heterotrophic respiration by ORC-STD are all much higher ($1 \sim 2$ times) than the measurement. As all the unburned biomass enter into litter pool immediately after fire, the heterotrophic respiration simulated by ORC-STD surges to unrealistically high level of $6000\,\mathrm{g\,C\,m^{-2}\,yr^{-1}}$, rendering the ecosystem an extremely big carbon source of $6000\,\mathrm{C\,m^{-2}\,yr^{-1}}$ (compared with measurement NEP of $-150\,\mathrm{C\,m^{-2}\,yr^{-1}}$ by Goulden et al., 2011 and $-202 \pm 53\,\mathrm{C\,m^{-2}\,yr^{-1}}$ by Randerson et al., 2006). In contrast, results by ORC-FM-NONSAG and GPPCAL-CMCD simulations agree more closely with measurements.

There is no difference in simulated GPP and total biomass carbon between ORC-FM-NOSNAG and GPPCAL-CMCD simulations. Within ~ 20 yr after fire, simulated heterotrophic respiration by ORC-FM-NOSNAG is slightly higher than GPPCAL-CMCD, which is an expected result as all the unburned biomass turns into litter immediately after fire in ORC-FM-NOSNAG simulation and contributes to heterotrophic respiration.

BGD
10, 7299–7366, 2013

3.2 Simulated fire carbon emissions

The simulated fire carbon emissions in the most recent fire events for the three site clusters for GPPCAL-CMCD simulation are: for Saskatchewan $3.12 \pm 1.3\,kg\,C\,m^{-2}$, for Manitoba $1.03 \pm 0.17\,kg\,C\,m^{-2}$, and for Alaska $0.53 \pm 0.03\,kg\,C\,m^{-2}$ (Table 5). The mean fire carbon emissions among all the 13 study sites are $1.40 \pm 1.15\,kg\,C\,m^{-2}$, with $0.33\,kg\,C\,m^{-2}$ being emitted from crown burning and $1.06\,kg\,C\,m^{-2}$ from surface burning. The mean fire carbon emission among 13 sites is very close to the average fire carbon emissions of $1.2\,kg\,C\,m^{-2}$ for central Canadian boreal forests fires that were recorded in Canadian Large Fire database, as reported by Amiro et al. (2001).

3.3 Evaluation of simulated annual GPP, TER and NEP

Simulated annual GPP, TER and NEP in comparison with EC measurements are shown in Fig. 6. Model outputs are shown for simulations both before (CNT-CMCD and CNT-HHCD) and after (GPPCAL-CMCD and GPPCAL-HHCD) multi-year average GPP assimilation. Note in the GPPCAL simulations, only the average multi-year GPP from the model is optimized to the measured mean value, so that the simulated inter-annual variability of GPP can still be compared against EC data.

In the CNT-CMCD simulation without GPP nudging, both GPP and TER are overestimated by the model across all study sites (Table 6, Fig. 6a) by approximately 30 %. No overestimation shows for NEP in CNT-CMCD simulation (Table 6, Fig. 6a), suggesting compensation of GPP and TER biases in NEP. In the CNT-HHCD simulation, the RTO regression slopes for GPP and TER are not significantly different from 1, indicating no systematic bias in simulation of these two carbon fluxes. Whereas NEP in CNT-HHCD is significantly lower than measurement values (~ 85 % by RTO slope). This shows that the choice of climate forcing data (low vs. high frequency) affects strongly the model-data misfit.

For CNT-CMCD simulation, the simulated to observed multi-year average GPP ratios are different depending on three clusters of evaluation sites. This ratio is 1.15 ± 0.27 for

BGD
10, 7299–7366, 2013

Saskatchewan sites, 1.42 ± 0.17 for Manitoba sites, and 2.13 ± 0.13 for Alaska sites. Simulated GPP tends to be overestimated by a larger extent when latitude increases.

Because the GPPCAL-CMCD and GPPCAL-HHCD runs use the same nudged GPP, the model-measurement metrics for annual GPP are the same for these two simulations (Table 6). As expected, nudging multi-year average GPP greatly improves the model-measurement agreement for annual GPP, with RTO regression slope equal to 1, and RMSD being reduced by more than ∼ 70 % compared to the non-assimilated runs (Table 6). Nudging GPP simultaneously improves the TER simulation in both GPPCAL-CMCD and GPPCAL-HCDD simulations. Model-measurement agreement for NEP in GPPCAL-HHCD is also improved after assimilation (RTO regression slope changes from 0.13 to 0.85, RMSD is reduced by more than half; Table 6), but NEP remains underestimated (too small modeled carbon sink) in GPPCAL-CMCD.

3.4 Evaluation of postfire evolution of LAI, biomass, forest floor, woody debris, and mineral soil organic carbon

In this section, the evaluations of ORCHIDEE_FM_BF output against biometric measurements are presented for LAI, biomass carbon, forest floor carbon, woody debris and soil carbon (Table 7). Note that the two GPP calibration simulations only differ for the EC observation period and carbon stocks are not expected to change greatly during these few years, thus the simulation results from the GPPCAL-CMCD simulation are used for comparison.

3.4.1 Leaf area index

RTO regression slope between simulated and measured LAI indicates that model underestimates LAI by an overall fraction of 24 % (RTO regression equal to 0.76, see Table 7) when all sites are considered together. The LAI in dry sites is underestimated by ∼ 30 % by the model and wet sites overestimated by 15 % (Table 7). The overlapping ratio between simulated and measured data is 0.43, indicating 43 % of measurements

BGD
10, 7299–7366, 2013

are well simulated by the model. A close look at the model – measurement data shows that LAI in the Manitoba dry sites have been underestimated by 50 % in the middle-aged forest (~ 80 yr) and by 30 % in the old-aged forest (~ 150 yr) (Fig. 7).

3.4.2 Total and aboveground biomass

With the re-growing of the forest stand after fire, forest biomass carbon is modeled to increase continuously with forest age (Fig. 8). The RTO regression slope for all dry and wet sites combined is not significantly different from 1, indicating a very good overall model-measurement agreement. Yet for wet sites, modeled biomass carbon is found to be overestimated by about 50 %, with a larger systematic RMSD than unbiased RMSD, likely because ORCHIDEE_FM_BF does not have sufficient limitation of growth for wet sites.

3.4.3 Forest floor carbon

RTO regression analysis indicates that forest floor carbon is underestimated by ~ 50 %, when pooling all study sites together (Table 7), explaining the bigger RMSD than unbiased RMSD. But due to the large uncertainty in the measurement data (Fig. 9), the overlapping ratio between simulated and measurement data is 0.43, which is moderately good (43 % of the measurements are reproduced by the model).

If the three clusters of sites are examined separately, some additional biases are revealed. For the Manitoba sites, forest floor carbon is found to be underestimated by the model, mainly in very young forest (< 10 yr) and forest older than ~ 70 yr. For Saskatchewan sites, oppositely, there is a very strong overestimation by the model (by a factor of 3) for forest floor carbon, although this result could probably be biased by the very scarce measurements.

BGD
10, 7299–7366, 2013

3.4.4 Woody debris

Model-measurement comparisons for woody debris, including standing dead wood (SDW), downed woody debris (DWD) and total woody debris (TWD), are shown in Fig. 10. The RTO regression slopes between simulated and measured woody debris for dry, wet and for all sites combined are 0.31, 0.30 and 0.50 respectively, suggesting underestimation by the model. The overlapping ratio is 0.43, indicating moderate model-measurement agreement. For dry sites and all sites combined, the systematic RMSD is bigger than unbiased RMSD, indicating a persistent model bias. But for wet sites, this bias is reduced and becomes smaller than unbiased RMSD.

At Manitoba sites, simulated SDW carbon is higher than field measurements for young forests (< 20 yr) (Fig. 10a). Note for both downed woody debris and total woody debris, the measurements are extremely high in forests around 20 yr old. This is because there is a delay in time in tree mortality after fire (Bond-Lamberty and Gower, 2008), whereas in the model, unburned tree biomass is considered to become standing dead wood immediately after fire.

3.4.5 Mineral soil organic carbon

The simulated mineral soil organic carbon begins to increase since the start of the simulation, and is still increasing slowly ($\sim 0.002\,\mathrm{kg\,C\,m^{-2}\,yr^{-1}}$) when the simulation reaches the postfire simulation after the most recent fire events. And there is only slight change over the postfire period after the most recent fire events (data not shown). Figure 11 shows the mean simulated mineral soil carbon over the postfire period, further averaged among sites, in comparison with measurement data. Our aim is to compare the simulated mineral soil carbon with collected measurement data in a qualitative way rather than to examine the postfire temporal evolution (as opposed with the comparison for other variables in this section). For this reason, the metrics in Sect. 2.5 used for quantitative model-measurement comparison with a focus on postfire temporal evolution is not applicable.

BGD
10, 7299–7366, 2013

The simulated mineral soil carbon agrees best with the well-drained measurements, and is generally smaller than the poorly drained measurements. For Saskatchewan, the simulated mineral soil carbon is ~2 times of the measured well-drained sites, while in Alaska, the simulated mineral soil carbon stock is half of the well-drained sites. Therefore, ORCHIDEE_FM_BF only has moderate to low capabilities to reproduce soil carbon, as it does not fully include decomposition processes (for example, the permafrost influence and cold historical temperature) that affect boreal soils. This variable can either be under- or overestimated by a factor of two across sites, although the spatial heterogeneity of mineral soil carbon in boreal forests is also great due to factors including soil drainage, nutrients availability, soil freezing and vegetation type (Gower et al., 1997).

As ORCHIDEE_FM_BF uses a three-pool model with different turnover rates to simulate mineral soil carbon, the discrepancy of mineral soil carbon between model simulation and measurement rather has rather only a relatively small contribution to the simulated carbon fluxes, as the discrepancy in C stocks mainly arises from the soil carbon pool with a low turnover rate. ORCHIDEE_FM_BF includes the effect of soil texture on mineral soil carbon decomposition, and soils with coarser texture (high sand and low clay content) have a faster decomposition rate and thus a lower soil carbon stock. Of the simulation sites in Manitoba (CA-NS1 to CA-NS7), the site CA-NS1 is clay-rich (sand : silt : clay = 0.02 : 0.13 : 0.86) and CA-NS7 is sand-rich (sand : silt : clay = 0.27 : 0.31 : 0.42). The simulated mineral soil carbon stock is 12.6 kg C m^{-2} for CA-NS1 and 4.7 kg C m^{-2} for CA-NS7. And the difference mainly resides in the slow pool of mineral soil carbon (see Sect. 2.2 for model description), and this difference results in a 16 % difference in heterotrophic respiration (data not shown).

3.5 Evaluation of modeled stand structure

One particularly interesting feature of ORCHIDEE_FM_BF is that the model equations represent the forest self-thinning process explicitly by comparing each year the theoretical maximum tree density (through quadratic mean diameter – maximum individual

BGD
10, 7299–7366, 2013

density curve) with modeled tree density. The default parameters for the self-thinning curve for European forests are used in this study (Bellassen et al., 2010) which predict the tree density within 20 % of that predicted by the relationship that is derived by using local observations (Newton, 2006).

The initial density for all study sites is set as 12 500 trees ha^{-1} for the young saplings after fire according to Wang et al. (2003). Simulated stand density, stand basal area (BA) and mean diameter at breast height (DBH) are compared with measurements in Fig. 12. Simulated stand density is found to agree best with observations at the Manitoba dry sites (Fig. 12a). For the young forest (< 40 yr) at wet sites and Alaska sites, stand density is overestimated by the model. The overlapping ratio between modeled and measurement data was 0.27, with the RMSD dominated by unbiased RMSD. For BA and DBH, none of the RTO regression slopes is significantly different from 1, indicating a good model-measurement agreement. The model-measurement overlapping ratios are 0.50, 0.33 for DBH and BA respectively.

3.6 Overall model performance across different soil drainage conditions

When examining model-measurement agreement for different soil drainage conditions, in terms of RTO regression goodness of fit (adjusted R^2), overlapping ratio, and RMSD, the model is found to perform better at dry sites than in wet sites for LAI, biomass carbon stock, DBH, stand density and basal area (5 out of 6 variables for which the comparison is applicable). This indicates the model has a general better performance in dry sites than wet ones.

Model-measurement agreement metrics across all evaluation sites for carbon fluxes and carbon stocks are summarized in Table 8, together with measurement accuracy. The average model-measurement overlapping ratio for LAI, biomass, forest floor and total woody debris carbon was 42 %. Except for forest floor carbon, the model-measurement RMSDs for all variables in Table 8 are lower than or equal to the uncertainty of field measurement, indicating that the model performance is on average satisfactory, given uncertainty in evaluation data.

BGD
10, 7299–7366, 2013

4 Discussion

In the preceding sections, the ORCHIDEE_FM_BF model is evaluated against chronosequence measurements of carbon fluxes, ecosystem carbon pools and stand structure, with focus on the capability of the model to reproduce the temporal evolution of each variable as a function of time after fire. To our knowledge, this is the first study that tries to evaluate a global process-based vegetation model for fire disturbances against multiple sites and multiple observation data stream. Although we trust the chronosequence stands are often carefully selected to make them comparable and thus representing the process of forest development, there are still site specific conditions which lead to spatial heterogeneity among sites and complicate model-measurement comparison. So the discussion below will focus on the more general issues on model-measurement comparison rather than explaining why some specific site or variable is overestimated or underestimated by the model.

4.1 Model improvement chain and simulated fire carbon emissions

In this study, we adapted ORCHIDEE_FM to ORCHIDEE_FM_BF to simulate stand-replacing fires and the postfire forest regrowth because we found that the standard version of ORCHIDEE and unmodified ORCHIDEE_FM did not perform sufficiently well for our evaluation purpose. Compared with standard version ORCHIDEE, ORCHIDEE_FM_BF greatly improves the model-measurement agreement for the four variables examined (GPP, NEP, heterotrophic respiration and total biomass carbon).

It is a bit surprising that that adding the snag process does not lead to significant improvement in model-measurement agreement in terms of postfire NEP trajectory shortly after fire (inset plot in Fig. 5b). This reflects the complexity of modeling, and may indicate the role of other process that are still missing in the model, including for example the respiration of snags. Beside, the model assumed a first order kinetic function with time to simulate snag falling and mixing with litter, while in reality the timing of snags entering decomposition is highly variable. Hilger et al. (2012) further

BGD
10, 7299–7366, 2013

demonstrated that the mass transfer rate between snags and litter differed from the snag falling rate which was derived by tree number counting.

A detailed and more accurate simulation of snag related heterotrophic process requires more measurement data that include for example both the postfire snag and litter amount as well as all the component of carbon fluxes (GPP, NPP, heterotrophic respiration with distinction made in soil and litter component), which is beyond the scope here. Nevertheless, the inclusion of the snag pool in the model allows the direct comparison of this carbon stock with measurement, and makes the model being able to represent one of the important long-term carbon stocks after fire (Manies et al., 2005).

Randerson et al. (2006) reported the total fire carbon emission of 1.56 $kgCm^{-2}$ for the site US-Bn3 (which burned in 1999). Kasischke and Hoy (2012) reported fire carbon emissions of 3.01 $kgCm^{-2}$ during large fire years and 1.69 $kgCm^{-2}$ during small fire years for Alaskan boreal froests. Our simulated fire carbon emissions of 0.53 $kgCm^{-2}$ for the three sites in Alaska are therefore smaller than these value. de Groot et al. (2009) reported surface fire carbon emissions for several wildfire events in Canada to range from 0.95 to 2.95 $kgCm^{-2}$ (assuming a 0.5 carbon fraction in the fuel), with an average of 1.1 $kgCm^{-2}$. Our simulated total fire carbon emissions for Manitoba sites are close to this estimation, and higher at the Saskatchewan sites.

Several studies point out that surface fuel combustion fraction contributes to biggest uncertainty in estimating fire carbon emissions from boreal forest fires (French et al., 2004; de Groot et al., 2009). Thus the difference in our simulated fire carbon emissions with that reported by others might be due to the simplified burning combustion fractions used in this study. The error in simulated fuel load could also contributes. As shown in Sect. 3.4.3, the forest floor carbon is generally underestimated by the model at the Alaska sites and overestimated at the Saskatchewan sites. This could partly explain the underestimation and overestimation in fire carbon emissions, in the two site clusters respectively. Nevertheless, when averaged across all the 13 study sites, the simulated fire carbon emissions are close to regional average carbon emissions

BGD
10, 7299–7366, 2013

of 1.2 kg C m^{-2} estimated by Amiro et al. (2001), implying a generally good across-site model-measurement agreement.

4.2 Effect of nudging observed multi-annual average GPP on improving other CO_2 fluxes

In the GPPCAL-CMCD and GPPCAL-HHCD simulations, the observed multi-year average GPP is "assimilated" (nudged) into the model to systematically correct simulated GPP. The simulated GPP is generally overestimated before nudging, confirming the "over-production" of ORCHIDEE that is already reported by Huntzinger et al. (2012) in the model intercomparison study for North America. This over-production is more prominent in low temperature regions, which is probably due to insufficient limitation on photosynthesis by low temperature.

It is clear that GPP assimilation improves the model-measurement fit for both annual GPP and TER (Sect. 3.3). The NEP simulation after GPP nudging is improved in GPPCAL-HHCD, but degraded in GPPCAL-CMCD (see Table 6). This is because NEP is the difference between two gross fluxes, and improving a first order bias in the gross fluxes does not always guarantee a more realistic simulation of annual NEP, because gross flux biases on GPP and TER partly cancel each other in the simulation of NEP.

Compared with GPPCAL-CMCD simulation, GPPCAL-HHCD has better agreement with observations in terms of both TER and NEP, with regression slopes closer to 1 and smaller systematic RMSD. This is reasonable as in case of observed GPP assimilation, GPP could be considered as being reasonably "true", and TER and accordingly NEP are thus mainly influenced by the difference in climate forcing data. As CMCD is monthly data from nearby meteorological stations completed by gridded CRU data (which needs to be converted into 30 min step before feeding into the model), it is supposed to be less realistic than the HHCD climate data which is obtained by in-situ measurement on flux sites with 30 min time step. This explains the

BGD
10, 7299–7366, 2013

better model-measurement agreement in GPPCAL-HHCD simulation, and the similar result has also been reported by Zhao et al. (2012).

However, the HHCD climate data are only available for the EC observation period, and are not suitable for spinup simulation as the simulated long term state of the ecosystem might be biased due to very few years of climate data being used. For this reason, the GPPCAL-HHCD run is designed mainly for model evaluation against CO_2 fluxes data. The rest of evaluations for carbon stocks are conducted using the GPPCAL-CMCD simulation instead, in which historical measured monthly climate data are used and supposed to reflect more realistically the historical state of the ecosystem being simulated. The GPPCAL-CMCD simulation is not as good as GPPCAL-HHCD for CO_2 fluxes, but still sufficient because carbon pools are less sensitive than fluxes to the difference of forcing data for only few years of the EC observation period.

In summary, GPP assimilation improved the model-data agreement for all CO_2 fluxes, indicating that correcting the GPP bias has already reduced the TER and NEP bias. Besides, the RMSDs for all sites combined for the carbon pools and stand structure variables have been reduced by 1–40 % in GPPCAL-CMCD simulation compared with CNT-CMCD simulations (RMSDs for CNT-CMCD simulations not shown). However, an accurate simulation of NEP was found to be more difficult to obtain than for GPP and TER, and comparison of 30 min with monthly forcing runs revealed significant model output biases of NEP due to forcing biases, a source of model error that was already noticed by Zhao et al. (2012) and Lin et al. (2011).

4.3 Attributing the role of past climate and CO_2 trends in the postfire evolution of carbon fluxes

Three simulations with different combinations of CO_2 and climate scenarios, namely varying CO_2 with varying climate (GPPCAL-CMCD), fixed CO_2 with varying climate (CO_2FIX-CLIMVAR), and fixed CO_2 with fixed climate (CO_2FIX-CLIMFIX), were conducted to attribute the different roles of the atmospheric CO_2 and varying climate in postfire forest CO_2 fluxes trajectory. GPPCAL-CMCD simulations were done for all the

BGD
10, 7299–7366, 2013

13 study sites. CO_2FIX-CLIMFIX and CO_2FIX-CLIMVAR simulations were done only for sites CA-NS1, CA-SF1, and US-Bn1 (see Sect. 2.4.4 for more detailed description).

The postfire GPP, TER and NEP trajectory for the three simulations are shown in Fig. 13 in comparison with eddy-covariance observations. The attribution analysis is only done for the period after the most recent fire events, the same period as the chronosequence study on each cluster of sites. So note for the site CA-NS1, it could be considered that the attribution analysis covers the whole fire cycle length as the chronosequence length (155 yr) is relatively long enough to cover the period of past atmospheric CO_2 increase. While for site CA-SF1 and US-Bn1, the attribution analysis covers rather short periods (for CA-SF1 28 yr, for US-Bn1 83 yr) and is intended to provide some insights that could not be easily obtained by the field observations.

When attributing the effects of varying CO_2 and climate for the site CA-NS1 (Manitoba), we assume that the simulation result by CO_2FIX-CLIMFIX for the time before 1968 (the starting year of meteorological station observation) followed the same curve by CO_2FIX-CLIMVAR. This is mainly due to the restriction in the availability of historical climate data on the meteorological station and this assumption may lead to underestimated varying climate effects as the climate trend before 1968 is not taken into account. For clarity, we focus the discussion on the site CA-NS1 and then briefly discuss the sites CA-SF1 and US-Bn1.

First, we find that the temporal pattern and magnitudes of postfire CO_2 fluxes in Manitoba sites (CA-NS1 to CA-NS7) over the past 150 yr are greatly driven by the fertilization effect of increasing atmospheric CO_2. The eddy-covariance measured magnitudes of postfire GPP for different ages of forest after fire are much higher than the simulation result with fixed CO_2 (CO_2FIX-CLIMVAR). *The GPP measurements can only be reproduced by the model when accounting for the effect of increasing* CO_2 (GPPCAL-CMCD, Fig. 13 upper-left panel). The same also applies for TER (Fig. 13 middle-left panel) and NEP (Fig. 13 lower-left panel), although the slight underestimation of NEP (carbon sink underestimated) by the GPPCAL-CMCD simulation is again shown (as shown in Fig. 6b). When comparing GPPCAL-CMCD and CO_2FIX-CLIMVAR simulations,

BGD
10, 7299–7366, 2013

accounting for the effect of rising CO_2 leads to both an increase in GPP and TER and a net increase in NEP (postfire carbon sink) (Table 9).

All three fluxes of GPP, TER and NEP are higher for the CO_2FIX-CLIMFIX simulation than CO_2FIX-CLIMVAR, *indicating that recent climate trends alone decrease the postfire carbon sequestration in our model simulation.* GPP is decreased by a bigger extent than TER when climate varies with CO_2 being fixed, causing a net decrease in NEP (Table 9). In summary, in terms of mean annual NEP over the entire postfire period for the site CA-NS1 (155 yr), increasing CO_2 caused an increase of 30.5 $g C m^{-2} yr^{-1}$ in mean annual NEP but climate trends alone a decrease by 3.5 $g C m^{-2} yr^{-1}$, with their combined effect as an increase of mean annual NEP by 26.9 $g C m^{-2} yr^{-1}$ (Table 9). For the period after the most recent fire event, the GPPCAL-CMCD (varying CO_2 with varying climate) simulates strong carbon sink in all the carbon stock compartments (total biomass, aboveground litter, belowground litter and mineral soil organic carbon) in the forest and accumulated NEP is 4.6 times higher than the carbon emissions in the fire (see Tables S1, S2 and S3 for the carbon budget for the three simulations at the three sites in the Supplement).

The role of varying CO_2 and climate in postfire carbon fluxes trajectory for the sites CA-SF1 and US-Bn1 is similar as that for CA-NS1, with increasing CO_2 playing a positive role and varying climate a negative one. In terms of mean annual NEP over the period after the most recent fire event for CA-SF1 (28 yr), increasing CO_2 caused an increase in NEP by 54.1 $g C m^{-2} yr^{-1}$ while varying climate resulted in a decrease by 22.8 $g C m^{-2} yr^{-1}$, with their combined effect to increase mean annual NEP by 31.2 $g C m^{-2} yr^{-1}$ (Table 9). For US-Bn1 (83 yr), increasing CO_2 caused an increase of 7.0 $g C m^{-2} yr^{-1}$ in mean annual NEP while varying climate a decrease by 7.5 $g C m^{-2} yr^{-1}$, with their combined effect to decrease mean annual NEP by 0.6 $g C m^{-2} yr^{-1}$ (Table 9).

The negative effect of climate trends in reducing postfire CO_2 uptake might be due to increasing water stress, probably caused by increase in temperature with the absence of sufficient increase in precipitation. Over the meteorological station observation

BGD
10, 7299–7366, 2013

period, mean annual temperature increased unanimously on the three site clusters, with 0.6 °C decade^{-1} in Alaska, 0.4 °C decade^{-1} in Manitoba and 0.3 °C decade^{-1} in Saskatchewan. The decadal trends in annual precipitation over the same period were 2.8 mm in Alaska, −14 mm in Manitoba and 7.7 mm in Saskatchewan. Of all the three regions, simulated soil moisture is lower in CO_2FIX-CLIMVAR than CO_2FIX-CLIMFIX (data not shown), indicating with the climate trend, plants tend to have more water stress. Thus the negative effect on forest NEP of varying climate indicated by model simulation might be due to increasing drought which is mainly caused by increasing temperature, which has also been reported by, for example, Michaelian et al. (2011) and Ma et al. (2012).

4.4 Model performance across different soil drainage conditions

One characteristic of boreal forest ecosystems is that ecosystem processes are greatly modulated by soil drainage conditions (Wang et al., 2003; Bond-Lamberty et al., 2006). Well-drained stands occur on flat upland or south-facing slopes and are often not underlain by permafrost. Poorly drained stands occur on flat lowland, or north-facing slopes and are generally underlain by continuous or discontinuous permafrost (Harden et al., 1997, 2001; Wang et al., 2003; Turetsky et al., 2011). Stands with poor soil drainage are often found to be associated with open canopy forests with relatively poor tree growth and low biomass, abundant bryophyte layer such as sphagnum (*Sphagnum* spp.) which typically grows in wet environments (Wang et al., 2003), frequently flooded soil, and massive amount of organic soil carbon due to the slow decomposition in the anaerobic environments (Bond-Lamberty et al., 2006).

ORCHIDEE_FM_BF is found to perform better in well-drained sites than in poorly drained ones. This is an expected result which could be explained by several key processes in the model. First, the soil hydrological processes in ORCHIDEE_FM_BF are simulated in a way that soil water drains away in forms of runoff or infiltration when excessive precipitation occurs (Ducoudré et al., 1993), which does not allow soil flooding. In reality, soils on poorly drained sites (either underlain by permafrost or due to

BGD
10, 7299–7366, 2013

topographic reason) tend to be saturated with water. In addition, the thick surface organic layer also functions to maintain moisture (Harden et al., 2006). These processes are however not included in ORCHIDEE_FM_BF. Second, in current versions of ORCHIDEE, the soil moisture always has a positive effect on photosynthesis (Krinner et al., 2005), which fails to represent the detrimental effect of excessive soil water on plant roots and negative effect on photosynthesis.

To improve model performance on poorly drained sites of a general process biogeochemical model such as ORCHIDEE, the poor drainage related hydrological and ecophysiological processes need to be incorporated into the model. These processes may include, for example, frequent soil flooding, detrimental effects of excessive soil water on root function and photosynthesis (Kreuzwieser et al., 2004), and reduced soil organic matter decomposition and nutrients mineralization (Wickland and Neff, 2007) in case of excessive soil moisture. Despite some valuable attempts (Bond-Lamberty et al., 2007a; Pietsch et al., 2003), the explicit process based modeling of forest with poor soil drainage or forested wetlands or peatland in general process biogeochemical models remains a big challenge.

Nevertheless, to examine the potential errors for regional application of ORCHIDEE_FM_BF on carbon fluxes and biomass carbon stocks, we tried to upscale the site level simulation errors from both good and poor drainage conditions (Table 7) to regional scale, by using the soil drainage distribution information in both Alaska and Canada. The soil drainage map for Alaska by Harden et al. (2001) shows that ~ 60 % of the soils were well-drained to moderately well-drained. For Canada, 65–75 % of the soils are well-drained and moderately well-drained (Soil Landscapes of Canada Working Group, 2010). To upscale the site level error to regional scale in a rather simple way, the RTO regression slopes for dry and wet sites (Table 7) are used together with dry/wet soil distribution to derive an area-weighted error. By this method, the model will probably generate an overestimation of total/above-ground biomass carbon stock by 12 % (Canada) to 18 % (Alaska), which is still within or comparable with the uncertainty

BGD
10, 7299–7366, 2013

of inventory-based net land-atmosphere carbon fluxes on national (Stinson et al., 2011) or regional scale (Hayes et al., 2012).

In summary, the model performance is found generally acceptable if all dry and wet sites are considered together. A process based generic model like ORCHIDEE-FM_BF should not be fine tuned at each study site for further reducing each error. Contrarily, only a multi-site agreement can be expected to assess for instance the model's capability to make regional simulations. Based on the results in Table 8, the key information is that the model-measurement error across multiple sites is comparable with the measurement accuracy, which justifies using the model for regional applications.

5 Summary and conclusion

In this study, we adapted a general purpose processbased global vegetation model ORCHIDEE to ORCHIDEE_FM_BF, to simulate stand-replacing fires in boreal forests and investigate postfire carbon dynamics during forest regrowth. Our study represents three advances considering the current general processbased biogeochemical modeling in boreal forests. First, ORCHDEE_FM_BF establishes a new forest cohort after crown fire disturbance, with explicit forest stand structure and self-thinning process, and is able to reproduce realistically key stand structure variables during forest regrowth. Second, the model simulation is done without requiring specific input from biometric measurements such as LAI, initial biomass etc, but is based on recurrent crown fire disturbances in a completely prognostic way. And surprisingly, both realistic fire carbon emissions and postfire ecosystem carbon dynamics are reproduced by the model.

Third, model evaluations are conducted by using multiple observations on multiple sites across different soil drainage conditions in North American boreal forest. Evaluation variables include carbon flux, carbon pools and stand forest stand structure. In particular, the carbon stock variables that are evaluated in this study include all the ecosystem carbon compartments (biomass, forest floor, woody debris and mineral soil)

BGD
10, 7299–7366, 2013

and thus make possible to evaluate the model performance on the whole ecosystem basis which allows the closure of the ecosystem carbon budget.

Despite lack of some important features in boreal forest ecosystem, such as poor drainage processes, permafrost layer, postfire nitrogen dynamics and bryophyte growth, the model is found generally being able to reproduce postfire forest carbon dynamics when errors are upscaled across multiple sites and different soil drainage conditions. The model calibration in this study will allow the regional carbon balance analysis for boreal forest by using a novel approach in which, the effects of standing-replacing fires are accounted in a spatially explicit way with a mosaic of different aged forest cohorts being established and simulated. And this will help to more accurately quantify the contribution of fires to historical and current carbon balance in boreal forests.

Supplementary material related to this article is available online at: http://www.biogeosciences-discuss.net/10/7299/2013/bgd-10-7299-2013-supplement.pdf.

Acknowledgements. This study was supported by the fire_cci project (http://www.esa-fire-cci.org/), funded by the European Space Agency. The authors would like to thank Shuhua Yi for providing the monthly climate data for the meteorological stations of Delta Junction and Fairbanks, Alaska. We thank Brian D. Amiro for providing the annual CO_2 flux data and the constructive comments which helps improving the manuscripts. We also thank Mike L. Goulden for providing carbon flux data on Manitoba sites. This work used eddy covariance data acquired by the FLUXNET community and in particular by the following networks: AmeriFlux (US Department of Energy, Biological and Environmental Research, Terrestrial Carbon Program (DEFG0204ER63917 and DEFG0204ER63911)), AfriFlux, AsiaFlux, CarboAfrica, CarboEuropeIP, CarboItaly, CarboMont, ChinaFlux, FluxnetCanada (supported by CFCAS, NSERC, BIOCAP, Environment Canada, and NRCan), GreenGrass, KoFlux, LBA, NECC, OzFlux, TCOS-Siberia, USCCC. We acknowledge the financial support to the eddy covariance data harmonization provided by CarboEuropeIP, FAO-GTOS-TCO, iLEAPS, Max Planck Institute for Biogeochemistry, National Science Foundation, University of Tuscia, Université Laval and

BGD
10, 7299–7366, 2013

Environment Canada and US Department of Energy and the database development and technical support from Berkeley Water Center, Lawrence Berkeley National Laboratory, Microsoft Research eScience, Oak Ridge National Laboratory, University of California Berkeley, University of Virginia.

The publication of this article is financed by CNRS-INSU.

References

Amiro, B. D., Todd, J. B., Wotton, B. M., Logan, K. A., Flannigan, M. D., Stocks, B. J., Mason, J. A., Martell, D. L., and Hirsch, K. G.: Direct carbon emissions from Canadian forest fires, 1959–1999, Can. J. Forest Res., 31, 512–525, 2001.

Amiro, B. D., Barr, A. G., Black, T. A., Iwashita, H., Kljun, N., McCaughey, J. H., Morgenstern, K., Murayama, S., Nesic, Z., Orchansky, A. L., and Saigusa, N.: Carbon, energy and water fluxes at mature and disturbed forest sites, Saskatchewan, Canada, Agr. Forest Meteorol., 136, 237–251, doi:10.1016/j.agrformet.2004.11.012, 2006.

Amiro, B. D., Barr, A. G., Barr, J. G., Black, T. A., Bracho, R., Brown, M., Chen, J., Clark, K. L., Davis, K. J., Desai, A. R., Dore, S., Engel, V., Fuentes, J. D., Goldstein, A. H., Goulden, M. L., Kolb, T. E., Lavigne, M. B., Law, B. E., Margolis, H. A., Martin, T., McCaughey, J. H., Misson, L., Montes-Helu, M., Noormets, A., Randerson, J. T., Starr, G., and Xiao, J.: Ecosystem carbon dioxide fluxes after disturbance in forests of North America, J. Geophys. Res., 115, G00K02, doi:10.1029/2010JG001390, 2010.

Anderson, R. S., Hallett, D. J., Berg, E., Jass, R. B., Toney, J. L., De Fontaine, C. S., and DeVolder, A.: Holocene development of Boreal forests and fire regimes on the Kenai Lowlands of Alaska, The Holocene, 16, 791–803, doi:10.1191/0959683606hol966rp, 2006.

BGD
10, 7299–7366, 2013

Balshi, M. S., McGuire, A. D., Zhuang, Q., Melillo, J., Kicklighter, D. W., Kasischke, E., Wirth, C., Flannigan, M., Harden, J., Clein, J. S., Burnside, T. J., McAllister, J., Kurz, W. A., Apps, M., and Shvidenko, A.: The role of historical fire disturbance in the carbon dynamics of the pan-boreal region: a process-based analysis, J. Geophys. Res.-Biogeo., 112, G02029, doi:10.1029/2006JG000380, 2007.

Balshi, M. S., McGuire, A. D., Duffy, P., Flannigan, M., Kicklighter, D. W., and Melillo, J.: Vulnerability of carbon storage in North American boreal forests to wildfires during the 21st century, Glob. Change Biol., 15, 1491–1510, 2009.

Bellassen, V., Le Maire, G., Dhôte, J. F., Ciais, P., and Viovy, N.: Modelling forest management within a global vegetation model – Part 1: Model structure and general behaviour, Ecol. Model., 221, 2458–2474, doi:10.1016/j.ecolmodel.2010.07.008, 2010.

Bond-Lamberty, B. and Gower, S. T.: Decomposition and fragmentation of coarse woody debris: re-visiting a boreal black spruce chronosequence, Ecosystems, 11, 831–840, doi:10.1007/s10021-008-9163-y, 2008.

Bond-Lamberty, B., Wang, C., and Gower, S. T.: Net primary production and net ecosystem production of a boreal black spruce wildfire chronosequence, Glob. Change Biol., 10, 473–487, 2004.

Bond-Lamberty, B., Gower, S. T., Goulden, M. L., and McMillan, A.: Simulation of boreal black spruce chronosequences: comparison to field measurements and model evaluation, J. Geophys. Res., 111, G02014, doi:10.1029/2005JG000123, 2006.

Bond-Lamberty, B., Gower, S. T., and Ahl, D. E.: Improved simulation of poorly drained forests using Biome-BGC, Tree Physiol., 27, 703–715, 2007a.

Bond-Lamberty, B., Peckham, S. D., Ahl, D. E., and Gower, S. T.: Fire as the dominant driver of central Canadian boreal forest carbon balance, Nature, 450, 89–92, doi:10.1038/nature06272, 2007b.

De Groot, W. J., Pritchard, J. M., and Lynham, T. J.: Forest floor fuel consumption and carbon emissions in Canadian boreal forest fires, Can. J. Forest Res., 39, 367–382, doi:10.1139/X08-192, 2009.

Ducoudré, N. I., Laval, K., and Perrier, A.: SECHIBA, a new set of parameterizations of the hydrologic exchanges at the land-atmosphere interface within the LMD Atmospheric General Circulation Model, J. Climate, 6, 248–273, doi:10.1175/1520-0442(1993)006<0248:SANSOP>2.0.CO;2, 1993.

BGD
10, 7299–7366, 2013

French, N. H. F., Kasischke, E. S., and Williams, D. G.: Variability in the emission of carbon-based trace gases from wildfire in the Alaskan boreal forest, J. Geophys. Res., 107, 8151, doi:10.1029/2001JD000480, 2002.
French, N. H. F., Goovaerts, P., and Kasischke, E. S.: Uncertainty in estimating carbon emissions from boreal forest fires, J. Geophys. Res., 109, D14S08, doi:10.1029/2003JD003635, 2004.
Goulden, M. L., Winston, G. C., McMillan, A. M. S., Litvak, M. E., Read, E. L., Rocha, A. V., and Rob Elliot, J.: An eddy covariance mesonet to measure the effect of forest age on land–atmosphere exchange, Glob. Change Biol., 12, 2146–2162, 2006.
Goulden, M., McMillan, A., Winston, G., Rocha, A., Manies, K., Harden, J., and Bond-Lamberty, B.: Patterns of NPP, GPP, respiration, and NEP during boreal forest succession, Glob. Change Biol., 17, 855–871, doi:10.1111/j.1365-2486.2010.02274.x, 2011.
Government of Canada, N.R.C.: Canadian Forest Service Publications: Fire behavior in immature jack pine, available at: http://cfs.nrcan.gc.ca/publications?id=22430, last access: 30 October, 2012.
Gower, S. T., Vogel, J. G., Norman, J. M., Kucharik, C. J., Steele, S. J., and Stow, T. K.: Carbon distribution and aboveground net primary production in aspen, jack pine, and black spruce stands in Saskatchewan and Manitoba, Canada, J. Geophys. Res., 102, 29029–29041, doi:10.1029/97JD02317, 1997.
Harden, J. W., O'Neill, K. P., Trumbore, S. E., Veldhuis, H., and Stocks, B. J.: Moss and soil contributions to the annual net carbon flux of a maturing boreal forest, J. Geophys. Res.-Atmos., 102, 28805–28816, doi:10.1029/97JD02237, 1997.
Harden, J. W., Trumbore, S. E., Stocks, B. J., Hirsch, A., Gower, S. T., O'Neill, K. P., and Kasischke, E. S.: The role of fire in the boreal carbon budget, Glob. Change Biol., 6, 174–184, 2000.
Harden, J. W., Meier, R., Silapaswan, C., Swanson, D. K., and Mcguire, A. D.: Soil drainage and its potential for influencing wildfires in Alaska, US Geological Survey Professional Paper, 139–144, 2001.
Harden, J. W., Manies, K. L., Turetsky, M. R., and Neff, J. C.: Effects of wildfire and permafrost on soil organic matter and soil climate in interior Alaska, Glob. Change Biol., 12, 2391–2403, doi:10.1111/j.1365-2486.2006.01255.x, 2006.

BGD
10, 7299–7366, 2013

Hayes, D. J., McGuire, A. D., Kicklighter, D. W., Gurney, K. R., Burnside, T. J., and Melillo, J. M.: Is the northern high-latitude land-based CO_2 sink weakening?, Global Biogeochem. Cy., 25, GB3018, doi:10.1029/2010GB003813, 2011.

Hayes, D. J., Turner, D. P., Stinson, G., McGuire, A. D., Wei, Y., West, T. O., Heath, L. S., De Jong, B., McConkey, B. G., Birdsey, R. A., Kurz, W. A., Jacobson, A. R., Huntzinger, D. N., Pa, Y., Post, W. M., and Cook, R. B.: Reconciling estimates of the contemporary North American carbon balance among terrestrial biosphere models, atmospheric inversions, and a new approach for estimating net ecosystem exchange from inventory-based data, Glob. Change Biol., 18, 1282–1299, doi:10.1111/j.1365-2486.2011.02627.x, 2012.

Hilger, A. B., Shaw, C. H., Metsaranta, J. M., and Kurz, W. A.: Estimation of snag carbon transfer rates by ecozone and lead species for forests in Canada, Ecol. Appl., 22, 2078–2090, doi:10.1890/11-2277.1, 2012.

Huntzinger, D. N., Post, W. M., Wei, Y., Michalak, A. M., West, T. O., Jacobson, A. R., Baker, I. T., Chen, J. M., Davis, K. J., Hayes, D. J., Hoffman, F. M., Jain, A. K., Liu, S., McGuire, A. D., Neilson, R. P., Potter, C., Poulter, B., Price, D., Raczka, B. M., Tian, H. Q., Thornton, P., Tomelleri, E., Viovy, N., Xiao, J., Yuan, W., Zeng, N., Zhao, M., and Cook, R.: North American Carbon Program (NACP) regional interim synthesis: Terrestrial biospheric model intercomparison, Ecol. Model., 232, 144–157, doi:10.1016/j.ecolmodel.2012.02.004, 2012.

Kane, E. S., Kasischke, E. S., Valentine, D. W., Turetsky, M. R., and McGuire, A. D.: Topographic influences on wildfire consumption of soil organic carbon in interior Alaska: implications for black carbon accumulation, J. Geophys. Res.-Biogeo., 112, G03017, doi:10.1029/2007JG000458, 2007.

Kasischke, E. S.: Boreal ecosystems in the global carbon cycle, in: Fire, Climate Change, and Carbon Cycling in the Boreal Forest, edited by: Kasischke, E. S. and Stocks, B. J., Springer, New York, 19–30, 2000.

Kasischke, E. S. and Hoy, E. E.: Controls on carbon consumption during Alaskan wildland fires, Glob. Change Biol., 18, 685–699, doi:10.1111/j.1365-2486.2011.02573.x, 2012.

Kasischke, E. S., Christensen, N. L., and Stocks, B. J.: Fire, global warming, and the carbon balance of boreal forests, Ecol. Appl., 5, 437–451, doi:10.2307/1942034, 1995.

Kasischke, E. S., O'Neill, K. P., French, N. H. F., and Bourgeau-Chavez, L. L.: Controls on patterns of biomass burning in Alaskan boreal forests, in: Fire, Climate Change, and Carbon Cycling in the Boreal Forest, edited by: Kasischke, E. S. and Stocks, B. J., Springer, New York, 173–196, 2000.

BGD
10, 7299–7366, 2013

Kreuzwieser, J., Papadopoulou, E., and Rennenberg, H.: Interaction of flooding with carbon metabolism of forest trees, Plant Biol., 6, 299–306, doi:10.1055/s-2004-817882, 2004.

Krinner, G., Viovy, N., De Noblet-Ducoudré, N., Ogée, J., Polcher, J., Friedlingstein, P., Ciais, P., Sitch, S., and Prentice, I. C.: A dynamic global vegetation model for studies of the coupled atmosphere–biosphere system, Global Biogeochem. Cy., 19, GB1015, doi:10.1029/2003GB002199, 2005.

Kurz, W. A. and Apps, M. J.: A 70-year retrospective analysis of carbon fluxes in the Canadian forest sector, Ecol. Appl., 9, 526–547, 1999.

Kurz, W. A., Dymond, C. C., White, T. M., Stinson, G., Shaw, C. H., Rampley, G. J., Smyth, C., Simpson, B. N., Neilson, E. T., Trofymow, J. A., Metsaranta, J. M., and Apps, M. J. : CBM-CFS3: A model of carbon-dynamics in forestry and land-use change implementing IPCC standards, Ecol. Model., 220, 480–504, doi:10.1016/j.ecolmodel.2008.10.018, 2009.

Lin, J. C., Pejam, M. R., Chan, E., Wofsy, S. C., Gottlieb, E. W., Margolis, H. A., and McCaughey, J. H.: Attributing uncertainties in simulated biospheric carbon fluxes to different error sources, Global Biogeochem. Cy., 25, GB2018, doi:10.1029/2010GB003884, 2011.

Litvak, M., Miller, S., Wofsy, S. C., and Goulden, M.: Effect of stand age on whole ecosystem CO_2 exchange in the Canadian boreal forest, J. Geophys. Res., 108, D38225, doi:10.1029/2001JD000854, 2003.

Liu, H. and Randerson, J. T.: Interannual variability of surface energy exchange depends on stand age in a boreal forest fire chronosequence, J. Geophys. Res., 113, G01006, doi:10.1029/2007JG000483, 2008.

Liu, H., Randerson, J. T., Lindfors, J., and Chapin, F. S.: Changes in the surface energy budget after fire in boreal ecosystems of interior Alaska: an annual perspective, J. Geophys. Res., 110, D13101, doi:10.1029/2004JD005158, 2005.

Ma, Z., Peng, C., Zhu, Q., Chen, H., Yu, G., Li, W., Zhou, X., Wang, W., and Zhang, W.: Regional drought-induced reduction in the biomass carbon sink of Canada's boreal forests, P. Natl. Acad. Sci. USA, 109, 2423–2427, doi:10.1073/pnas.1111576109, 2012.

Mack, M. C., Treseder, K. K., Manies, K. L., Harden, J. W., Schuur, E. A. G., Vogel, J., Randerson, J. T., and Chapin III, F. S.: Recovery of aboveground plant biomass and productivity after fire in mesic and dry black spruce forests of Interior Alaska, Ecosystems, 11, 209–225, doi:10.1007/s10021-007-9117-9, 2008.

BGD
10, 7299–7366, 2013

Manies, K. L. and Harden, J. W.: Soil Data from Different-Age *Picea mariana* Stands near Delta Junction, US Department of the Interior, US Geological Survey, Open-File Report 2011-1061, 4–5, 2011.
Manies, K. L., Harden, J. W., Silva, S. R., Briggs, P. H., and Schmid, B. M.: Soil Data from *Picea mariana* Stands near Delta Junction, Alaska of Different Ages and Soil Drainage Type, US Department of the Interior, US Geological Survey, Open-File Report 2004-1271, 4–5, 2004.
Manies, K. L., Harden, J. W., Bond-Lamberty, B. P., and O'Neill, K. P.: Woody debris along an upland chronosequence in boreal Manitoba and its impact on long-term carbon storage, Can. J. Forest Res., 35, 472–482, doi:10.1139/x04-179, 2005.
Manies, K. L., Harden, J. W., and Veldhuis, H.: Soil Data from a Moderately Well and Somewhat Poorly Drained Fire Chronosequence near Thompson, Manitoba, Canada, US, US Department of the Interior, US Geological Survey, Open File Report 2006-1291, 4–5, 2006.
McGuire, A. D., Anderson, L. G., Christensen, T. R., Dallimore, S., Guo, L., Hayes, D. J., Heimann, M., Lorenson, T. D., Macdonald, R. W., and Roulet, N.: Sensitivity of the carbon cycle in the Arctic to climate change, Ecol. Monogr., 79, 523–555, 2009.
Michaelian, M., Hogg, E. H., Hall, R. J., and Arsenault, E.: Massive mortality of aspen following severe drought along the southern edge of the Canadian boreal forest, Glob. Change Biol., 17, 2084–2094, doi:10.1111/j.1365-2486.2010.02357.x, 2011.
Newton, P. F.: Asymptotic size–density relationships within self-thinning black spruce and jack pine stand-types: parameter estimation and model reformulations, Forest Ecol. Manag., 226, 49–59, doi:10.1016/j.foreco.2006.01.023, 2006.
O'Donnell, J. A., Harden, J. W., McGuire, A. D., Kanevskiy, M. Z., Jorgenson, M. T., and Xu, X.: The effect of fire and permafrost interactions on soil carbon accumulation in an upland black spruce ecosystem of interior Alaska: implications for post-thaw carbon loss, Glob. Change Biol., 17, 1461–1474, doi:10.1111/j.1365-2486.2010.02358.x, 2011.
Pan, Y., Birdsey, R. A., Fang, J., Houghton, R., Kauppi, P. E., Kurz, W. A., Phillips, O. L., Shvidenko, A., Lewis, S. L., Canadell, J. G., Ciais, P., Jackson, R. B., Pacala, S. W., McGuire, A. D., Piao, S. L., Rautiainen, A., Sitch, S., and Hayes, D.: A large and persistent carbon sink in the world's forests, Science, 333, 988–993, doi:10.1126/science.1201609, 2011.
Parton, W., Stewart, J., and Cole, C.: Dynamics of C, N, P and S in grassland soils: a model, Biogeochemistry, 5, 109–131, doi:10.1007/BF02180320, 1988.

BGD
10, 7299–7366, 2013

Pietsch, S. A., Hasenauer, H., Kucera, J., and Cermák, J.: Modeling effects of hydrological changes on the carbon and nitrogen balance of oak in floodplains, Tree Physiol., 23, 735–746, 2003.

Pregitzer, K. and Euskirchen, E.: Carbon cycling and storage in world forests: biome patterns related to forest age, Glob. Change Biol., 10, 2052–2077, 2004.

Randerson, J. T., Liu, H., Flanner, M. G., Chambers, S. D., Jin, Y., Hess, P. G., Pfister, G., Mack, M. C., Treseder, K. K., Welp, L. R., Chapin, F. S., Harden, J. W., Goulden, M. L., Lyons, E., Neff, J. C., Schuur, E. A. G., and Zender, C. S.: The impact of boreal forest fire on climate warming, Science, 314, 1130–1132, doi:10.1126/science.1132075, 2006.

Seiler, W. and Crutzen, P. J.: Estimates of gross and net fluxes of carbon between the biosphere and the atmosphere from biomass burning, Climatic Change, 2, 207–247, doi:10.1007/BF00137988, 1980.

Sitch, S., Smith, B., Prentice, I. C., Arneth, A., Bondeau, A., Cramer, W., Kaplan, J. O., Levis, S., Lucht, W., Sykes, M. T., Thonicke, K., and Venevsky, S.: Evaluation of ecosystem dynamics, plant geography and terrestrial carbon cycling in the LPJ dynamic global vegetation model, Glob. Change Biol., 9, 161–185, doi:10.1046/j.1365-2486.2003.00569.x, 2003.

Stinson, G., Kurz, W. A., Smyth, C. E., Neilson, E. T., Dymond, C. C., Metsaranta, J. M., Boisvenue, C., Rampley, G. J., Li, Q., White, T. M., and Blain, D.: An inventory-based analysis of Canada's managed forest carbon dynamics, 1990 to 2008, Glob. Change Biol., 17, 2227–2244, doi:10.1111/j.1365-2486.2010.02369.x, 2011.

Soil Landscapes of Canada Working Group: Soil Landscapes of Canada version 3.2. Agriculture and Agri-Food Canada, digital map and database at 1 : 1 million scale, available at: http://sis.agr.gc.ca/cansis/nsdb/slc/v3.2/index.html, last access: 7 February 2013, 2010.

Stocks, B. J.: Fire behavior in immature jack pine, Can. J. Forest Res., 17, 80–86, doi:10.1139/x87-014, 1987.

Stocks, B. J.: Fire behavior in mature jack pine, Can. J. Forest Res., 19, 783–790, doi:10.1139/x89-119, 1989.

Stocks, B. J., Mason, J. A., Todd, J. B., Bosch, E. M., Wotton, B. M., Amiro, B. D., Flannigan, M. D., Hirsch, K. G., Logan, K. A., Martell, D. L., and Skinner, W. R.: Large forest fires in Canada, 1959–1997, J. Geophys. Res.-Atmos., 108, 8149, doi:10.1029/2001JD000484, 2002.

BGD
10, 7299–7366, 2013

Trumbore, S. E. and Harden, J. W.: Accumulation and turnover of carbon in organic and mineral soils of the BOREAS northern study area, J. Geophys. Res., 102, 28817–28830, doi:10.1029/97JD02231, 1997.
Turetsky, M. R., Kane, E. S., Harden, J. W., Ottmar, R. D., Manies, K. L., Hoy, E., and Kasischke, E. S.: Recent acceleration of biomass burning and carbon losses in Alaskan forests and peatlands, Nat. Geosci., 4, 27–31, doi:10.1038/ngeo1027, 2011.
Wang, C., Bond-Lamberty, B., and Gower, S.: Carbon distribution of a well-and poorly-drained black spruce fire chronosequence, Glob. Change Biol., 9, 1066–1079, 2003.
Wang, T., Brender, P., Ciais, P., Piao, S., Mahecha, M. D., Chevallier, F., Reichstein, M., Ottlé, C., Maignan, F., Arain, A., Bohrer, G., Cescatti, A., Kiely, G., Law, B. E., Lutz, M., Montagnani, L., Moors, E., Osborne, B., Panferov, O., Papale, D., and Vaccari, F. P.: State-dependent errors in a land surface model across biomes inferred from eddy covariance observations on multiple timescales, Ecol. Model., 246, 11–25, doi:10.1016/j.ecolmodel.2012.07.017, 2012.
University of East Anglia Climatic Research Unit (CRU), Jones, P., and Harris, I.: CRU Time Series (TS) high resolution gridded datasets, NCAS British Atmospheric Data Centre, available at: http://badc.nerc.ac.uk/view/badc.nerc.ac.uk__ATOM__dataent_1256223773328276, last access: 5 March 2011, 2008.
van der Werf, G. R., Randerson, J. T., Giglio, L., Collatz, G. J., Kasibhatla, P. S., and Arellano Jr., A. F.: Interannual variability in global biomass burning emissions from 1997 to 2004, Atmos. Chem. Phys., 6, 3423–3441, doi:10.5194/acp-6-3423-2006, 2006.
van der Werf, G. R., Randerson, J. T., Giglio, L., Collatz, G. J., Mu, M., Kasibhatla, P. S., Morton, D. C., DeFries, R. S., Jin, Y., and van Leeuwen, T. T.: Global fire emissions and the contribution of deforestation, savanna, forest, agricultural, and peat fires (1997–2009), Atmos. Chem. Phys., 10, 11707–11735, doi:10.5194/acp-10-11707-2010, 2010.
Wickland, K. P. and Neff, J. C.: Decomposition of soil organic matter from boreal black spruce forest: environmental and chemical controls, Biogeochemistry, 87, 29–47, doi:10.1007/s10533-007-9166-3, 2007.
Yi, S., Manies, K., Harden, J., and McGuire, D.: Characteristics of organic soil in black spruce forests: implications for the application of land surface and ecosystem models in cold regions, Geophys. Res. Lett., 36, L05501, doi:10.1029/2008GL037014, 2009.
Zhao, Y., Ciais, P., Peylin, P., Viovy, N., Longdoz, B., Bonnefond, J. M., Rambal, S., Klumpp, K., Olioso, A., Cellier, P., Maignan, F., Eglin, T., and Calvet, J. C.: How errors on meteorologi-

BGD
10, 7299–7366, 2013

cal variables impact simulated ecosystem fluxes: a case study for six French sites, Biogeosciences, 9, 2537–2564, doi:10.5194/bg-9-2537-2012, 2012.

BGD
10, 7299–7366, 2013

Table 1. Measurement sites used in this study for model evaluation, their geographical coordinates, soil texture, pre-fire dominant vegetation species, year of the most recent fire event, and the period of eddy-covariance observation.

Site Name		Lat	Lon	Soil texture[a]			Pre-fire dominant species[b]	Year of burn	OSY[c]	OEY[c]
				Sand	Silt	Clay				
Saskatchewan	CA-SF1	54.5	−105.8	0.58	0.32	0.1	Jack pine	1977	2003	2005
	CA-SF2	54.3	−105.9	0.58	0.32	0.1	Jack pine	1989	2003	2005
	CA-SF3	54.1	−106.0	0.58	0.32	0.1	Jack pine	1998	2003	2005
Manitoba	CA-NS1	55.9	−98.5	0.02	0.13	0.86	Black spruce	1850	2002	2005
	CA-NS2	55.9	−98.5	0.27	0.31	0.42	Black spruce	1930	2001	2005
	CA-NS3	55.9	−98.4	0.27	0.31	0.42	Black spruce	1964	2001	2005
	CA-NS4	55.9	−98.4	0.27	0.31	0.42	Black spruce	1964	2002	2004
	CA-NS5	55.9	−98.5	0.27	0.31	0.42	Black spruce	1981	2001	2005
	CA-NS6	55.9	−99.0	0.27	0.31	0.42	Black spruce	1989	2001	2005
	CA-NS7	56.6	−100.0	0.34	0.29	0.37	Black spruce	1998	2002	2005
Alaska	US-Bn1	63.9	−145.4	0.82	0.12	0.06	Black spruce	1920	2003	2003
	US-Bn2	63.9	−145.4	0.82	0.12	0.06	Black spruce	1987	2003	2003
	US-Bn3	63.9	−145.7	0.82	0.12	0.06	Black spruce	1999	2003	2003

[a] Soil texture information, where available, is provided by site PIs, otherwise is completed by soil map of Zobler (1986) and translated into sand/silt/clay fractions by the model default values that correspond to soil types in Zobler map.
[b] Black spruce: *Picea mariana* (Mill.) BSP; Jack pine: *Pinus banksiana* Lamb.
[c] OSY, Eddy covariance Observation period Start Year; OEY, Eddy covariance Observation period End Year.

BGD
10, 7299–7366, 2013

Table 2. Variables used for validation and their data sources.

Variable	Site	Evaluation data source
GPP, NEP, TER	Alaska Manitoba Saskatchewan	Amiro et al., 2010
Leaf area index	Manitoba Saskatchewan Alaska	Goulden et al., 2011; Wang et al., 2003; Bond-Lamberty and Gower, 2008 Mkabela et al., 2009 J. T. Randerson
Total biomass carbon	Manitoba	Wang et al., 2003; Goulden et al., 2011
Aboveground biomass carbon	Saskatchewan Alaska	Mkabela et al., 2009; Gower et al., 1999 J. T. Randerson; Mack et al., 2008
Woody debris carbon[a]	Manitoba	Bond-Lamberty and Gower, 2008; Wang et al., 2003; Mkabela et al., 2009
Forest floor carbon[b]	Manitoba Saskatchewan Alaska	Wang et al., 2003; Goulden et al., 2011; Harden et al., 2012 Gower et al., 1997 Yi et al., 2010; Harden et al., 2012
Mineral soil carbon[c]	Alaska Saskatchewan Manitoba	Yi et al., 2010 Mkabela et al., 2009; Harden et al., 2000
DBH, Individual density, and Basal Area	Manitoba Alaska	Wang et al., 2003 Mack et al., 2008

[a] Detailed definitions for woody debris carbon are provided in Sect. 2.5.1.

[b] Forest floor carbon includes litter, dead moss and fine woody detritus, in distinctive horizons depending on site conditions (Manies et al., 2004, 2006; Manies and Harden, 2011): L (Live moss, dead leaves, twigs, lichen, etc.), D (Dead moss), F (Fibric or fibrous organic layers), M (Mesic organic layers) and H (Humic or sapric organic layers).

[c] Mineral soil carbon measurements include three soil layers where present (Manies et al., 2006), A: soil that forms at the surface or below organic horizons with less than 20 percent organic matter; B: mineral soil that has formed below an A horizon with little or none of its original rock structure; C: mineral soil that has been little affected by pedogenic processes.

BGD
10, 7299–7366, 2013

Table 3. Detailed information for the use of composite monthly climate data in the climate forcing history.

Site Name	Period of meteorological station data availability	Climate forcing history			
		First spinup and the first 19 fire rotations of the second spinup*	20th fire rotation of the second spinup	Postfire simulation before the EC observation period	Simulation for EC observation period
CA-SF1	1943–2006	1943–76(avg)	1943–76(avg) + 1943–76	1977–2002	2003–2005
CA-SF2		1943–88(avg)	1943–88(avg) + 1943–88	1989–2002	2003–2005
CA-SF3		1943–97(avg)	1943–98(avg) + 1943–98	1998–2002	2003–2005
CA-NS1	1968–2006	1968–80(avg)	1968–80(avg)	1968–80(avg) + 1968–2001	2002–2005
CA-NS2		1968–80(avg)	1968–80(avg)	1968–80(avg) + 1968–2000	2001–2005
CA-NS3		1968–80(avg)	1968–80(avg)	1968–80(avg) + 1968–2000	2001–2005
CA-NS4		1968–80(avg)	1968–80(avg)	1968–80(avg) + 1968–2001	2002–2004
CA-NS5		1968–80(avg)	1968–80(avg)	1981–2000	2001–2005
CA-NS6		1968–88(avg)	1968–88(avg) + 1968–88	1989–2000	2001–2005
CA-NS7		1968–97(avg)	1968–98(avg) + 1968–98	1998–2001	2002–2005
US-Bn1	1930–2006	1930–59(avg)	1930–59(avg)	1930–59(avg) + 1930–2002	2003
US-Bn2		1930–86(avg)	1930–86(avg) + 1943–86	1987–2002	2003
US-Bn3		1930–98(avg)	1943–98(avg) + 1930–98	1999–2002	2003

* "avg" means the averaged monthly climate forcing data over the specified period.

BGD
10, 7299–7366, 2013

Table 4. List of simulations, and their climate and atmospheric CO_2 forcing.

Name	Model used	Climate forcing	CO_2 forcing[a]
CNT-CMCD	ORCHIDEE_FM_BF	CMCD	CO_2VAR
CNT-HHCD	ORCHIDEE_FM_BF	HHCD for only EC obs. period	CO_2VAR
GPPCAL-CMCD	ORCHIDEE_FM_BF	CMCD	–
GPPCAL-HHCD	ORCHIDEE_FM_BF	HHCD for only EC obs. period	–
CO_2FIX-CLIMVAR (only for sites CA-NS1, CA-SF1, US-Bn1)	ORCHIDEE_FM_BF	CMCD	CO_2FIX
CO_2FIX-CLIMFIX (only for sites CA-NS1, CA-SF1, US-Bn1)	ORCHIDEE_FM_BF	The same average CMCD as used for spinup runs[b]	CO_2FIX
ORC-STD	Standard ORCHIDEE with fire and without snag	CMCD	CO_2VAR
ORC-FM-NOSNAG	ORCHIDEE_FM with fire but without snag	CMCD	CO_2VAR

[a] Atmospheric CO_2 forcing for GPPCAL-CMCD and GPPCAL-HHCD simulations is not applicable because GPP is externally forced to the model in the simulation, by nudging mean multi-year observed annual GPP into the model.
[b] For the CO_2FIX-CLIMFIX simulation, the average monthly climate data used are: 1968–1980(avg) for CA-NS1, 1943–1976(avg) for site CA-SF1, and 1930–1959(avg) for site US-Bn1 (see also Table 3).

BGD
10, 7299–7366, 2013

Table 5. Simulated fire carbon emissions ($kg C m^{-2}$) from live biomass, aboveground litter, and total carbon emissions for the most recent fire event for the three site clusters by GPPCAL-CMCD simulation. Numbers show the mean values for each site cluster with standard deviation being shown in brackets.

Site cluster	Live biomass	Aboveground litter	Total carbon emissions
Saskatchewan	0.60 (0.15)	2.52 (1.22)	3.12 (1.35)
Manitoba	0.31 (0.06)	0.72 (0.12)	1.03 (0.17)
Alaska	0.12 (0.02)	0.41 (0.02)	0.53 (0.03)
Average	0.33 (0.18)	1.06 (0.98)	1.40 (1.15)

BGD
10, 7299–7366, 2013

Table 6. Model-measurement comparison metrics for annual GPP, TER and NEP. The left-hand (right-hand) column shows values before (after) nudging the observed multi-year GPP into the model (see Sect. 2.4.4 for more details).

Metrics considered	GPP	TER	NEP	GPP	TER	NEP
	CNT-CMCD			GPPCAL-CMCD		
Slope	1.28	1.29	0.79	1.00	1.05	0.41
Adjusted R^2	0.95	0.96	0.62	0.98	0.98	0.48
p value	0.00	0.00	0.06	1.00	0.05	0.00
RMSD	247	215	61	76	87	70
RMSD_sys	175	160	21	0	31	57
RMSD_unbias	174	143	57	76	81	39
	CNT-HHCD			GPPCAL-HHCD		
Slope	0.91	1.02	0.13	1.00	0.98	0.85
Adjusted R^2	0.84	0.92	−0.02	0.98	0.98	0.58
p value	0.19	0.76	0.00	1.00	0.31	0.24
RMSD	244	166	138	76	76	69
RMSD_sys	57	9	84	0	14	15
RMSD_unbias	237	166	110	76	74	67

Linear regression (of form $y = \text{slope} \cdot x$) is fitted between simulated and observed annual data across all evaluation sites. Sample size is 33 for GPP, and 31 for TER and NEP. Data reported here include regression slope, and the probability for the slope to be significantly not different from 1 (p value), adjusted goodness of fit (adjusted R^2, a modification of R^2 that adjusts for the number of explanatory variables), Root Mean Square Deviation (RMSD), systematic and unbiased RMSD (see Sect. 2.5.2 for detailed description). Tests with p value < 0.05 (i.e. slope $\neq 1$) are underlined for emphasis.

BGD
10, 7299–7366, 2013

Table 7. Model-measurements comparison metrics for LAI, biomass carbon, forest floor carbon, total coarse woody debris, diameter at breast height (DBH), stand individual density, and basal area (BA) (see Sect. 2.1 for the definition of the variables; see Sect. 2.5.1 for how modeled and field observation data were matched against each other for woody debris and forest floor).

Items	drainage	LAI	Biomass carbon	Forest floor carbon	Woody debris	DBH	Stand individual density	Basal Area
N	All	33	37	35	60	12	11	12
	Dry	26	27	26	53	7	6	7
	Wet	7	10	9	7	5	5	5
Slope	All	0.76	1.03	0.51	0.31	0.79	1.14	0.89
	Dry	0.71	0.94	0.54	0.3	0.74	1.06	0.76
	Wet	1.15	1.55	0.47	0.50	0.89	1.32	1.50
p value	All	0.00	0.69	0.00	0.00	0.06	0.54	0.43
	Dry	0.00	*0.37	0.00	0.00	0.02	*0.80	0.03
	Wet	0.48	0.02	0.00	0.24	0.70	0.56	0.25
Adjusted R^2	All	0.78	0.86	0.59	0.34	0.85	0.72	0.80
	Dry	0.79	*0.89	0.57	*0.37	*0.94	*0.81	*0.94
	Wet	0.85	0.89	0.66	0.23	0.77	0.64	0.82
Overlapping Ratio	All	0.43	0.38	0.43	0.43	0.50	0.27	0.33
	Dry	*0.47	*0.38	0.35	0.43	*0.57	*0.33	*0.43
	Wet	0.25	0.38	0.67	-	0.40	0.20	0.20
RMSD	All	1.13	1018	1884	2165	1.74	6595	8.57
	Dry	1.20	*865	*1810	2199	*1.52	*5481	*6.87
	Wet	0.86	1347	2083	1890	2.00	7723	10.50
RMSD_sys	All	0.58	69	1416	1839	0.93	1292	2.08
	Dry	0.74	152	1279	1933	1.25	656	5.36
	Wet	0.26	965	1763	900	0.42	2401	6.05
RMSD_unbias	All	0.98	1015	1242	1142	1.46	6467	8.31
	Dry	0.94	851	1281	1047	0.87	5441	4.30
	Wet	0.83	939	1111	1662	1.96	7340	8.58

See Sect. 2.5.2 for explanation for all items except N which means the sample size. p value < 0.05 are underlined for emphasis (which means regression slope is significantly from 1). Underlined RMSD_sys indicates that the value of RMSD_sys is bigger than RMSD_unbias, which means RMSD is dominated by systematic error and poor model-measurement agreement. Stars (*) indicate a better model-measurement agreement in dry sites than in wet sites. Woody debris includes all standing dead wood (STD), downed woody debris (DWD) and total woody debris (TWD).

BGD
10, 7299–7366, 2013

Table 8. Model-measurement RMSD, RTO regression slope, overlapping ratio for all sites combined, and measurement accuracy for GPP, TER, NEP, LAI, biomass carbon, total woody debris and forest floor carbon.

Variable	RMSD	RTO regression slope	Overlaping ratio	Measurement accuracy*
Gross primary production ($gCm^{-2}yr^{-1}$)	76	–	–	100
Total ecosystem respiration ($gCm^{-2}yr^{-1}$)	76	–	–	200
Net ecosystem production ($gCm^{-2}yr^{-1}$)	69	–	–	50
Leaf Area Index (m^2m^{-2})	1.13	0.76	0.43	2
Biomass carbon (gCm^{-2})	1018	1.03	0.38	1000
Woody debris (gCm^{-2})	1885	0.35	0.43	2000
Forest floor carbon (gCm^{-2})	1884	0.51	0.43	1000

*Measurement accuracy information is from Goulden et al. (2011). For GPP, TER and NEP, measurement and aggregation accuracy is used, and for other variables, across landscape sampling accuracy is used.

BGD
10, 7299–7366, 2013

Table 9. Effects of varying atmospheric CO_2 and climate and their combined effect on mean annual carbon fluxes ($g C m^{-2} yr^{-1}$) over the chronosequence study period after the most recent fire event. The respective postfire period length for the evaluation sites CA-NS1, CA-SF1 and US-Bn1 are 155, 28 and 83 yr.

Carbon flux		Effect on mean annual carbon flux over the chronosequencee period*			Simulated mean annual carbon flux over the chronosequence period		
		Climate trends	Rising CO_2	Combined	CO_2FIX-CLIMFIX	CO_2FIX-CLIMVAR	GPPCAL-CMCD
CA-NS1	GPP	−9.3	91.4	82.1	461.4	452.1	543.5
	TER	−5.8	61.0	55.2	454.0	448.2	509.2
	NEP	−3.5	30.5	26.9	7.4	3.9	34.3
CA-SF1	GPP	−35.8	201.7	165.9	681.0	645.2	846.9
	TER	−13.0	147.7	134.7	672.7	659.8	807.4
	NEP	−22.8	54.1	31.2	8.3	−14.6	39.5
US-Bn1	GPP	−31.8	35.1	3.3	230.7	198.9	234.0
	TER	−24.3	28.1	3.9	225.1	200.9	229.0
	NEP	−7.5	7.0	−0.6	5.6	−2.0	5.0

* Climate effect was calculated as difference between simulations of CO_2FIX-CLIMVAR and CO_2FIX-CLIMFIX, and CO_2 effect was calculated as difference between simulations of GPPCAL-CMCD and CO_2FIX-CLIMVAR, and combined effect as difference between simulations of GPPCAL-CMCD and CO_2FIX-CLIMFIX.

BGD
10, 7299–7366, 2013

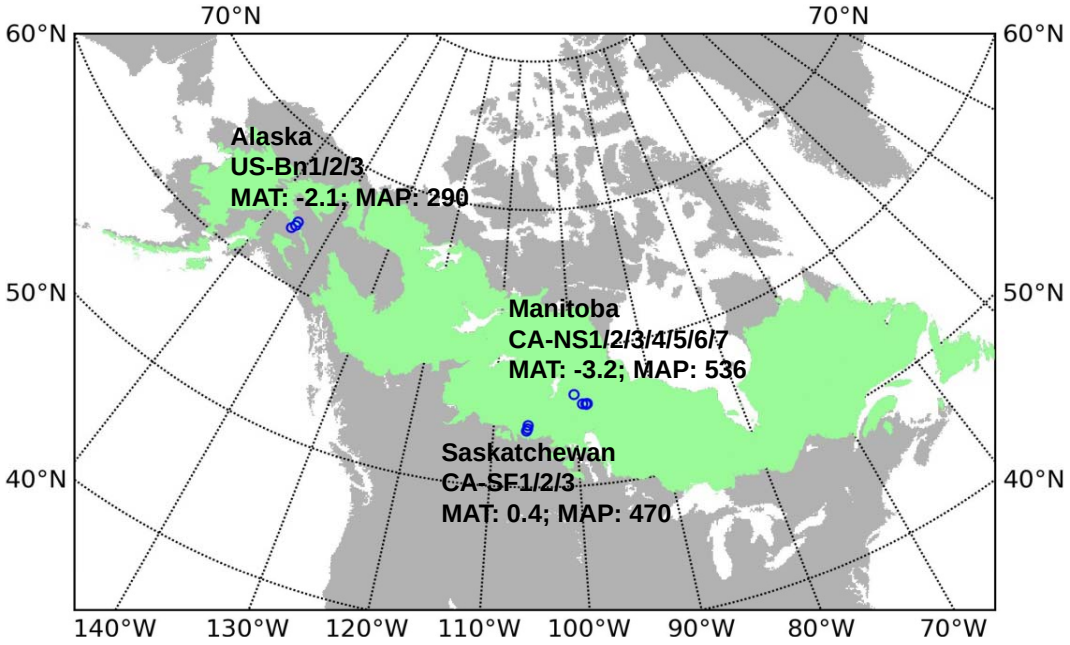

Fig. 1. Eddy-covariance measurement sites in North American boreal forests as disturbed by stand-replacing fire, used as evaluation sites in this study. Three sites (US-Bn1 to US-Bn3) are located in Alaska, seven sites (CA-NS1 to CA-NS7) in Manitoba, and three sites (CA-SF1 to CA-SF3) in Saskatchewan. The green belt shows the extent of the boreal forest biome. MAT, mean annual temperature (°C); MAP, mean annual precipitation (mm).

BGD
10, 7299–7366, 2013

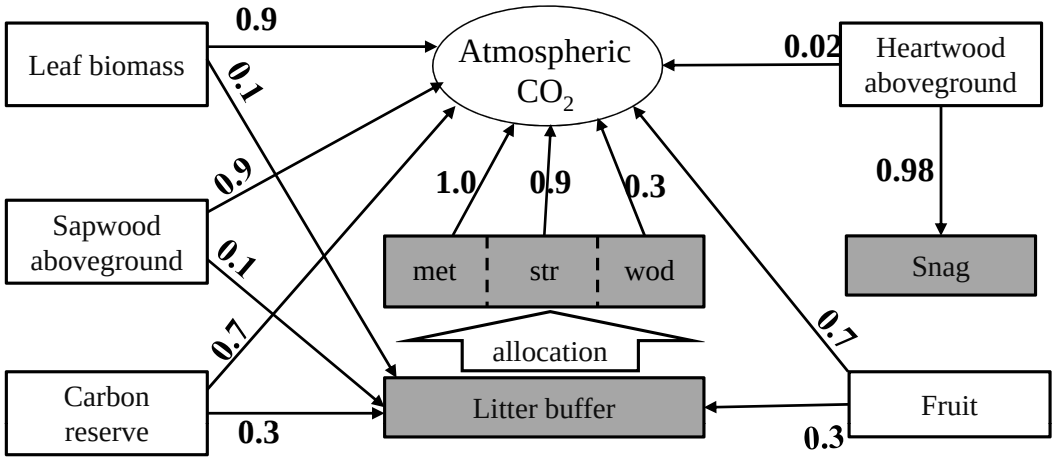

Fig. 2. Fire combustion fractions for various carbon pools, and transfer of unburned live biomass to litter and snag. Numbers in the figure means transferring fraction between different pools. Blank rectangles indicate biomass carbon pool and shaded rectangles indicate snag and litter pool. For the three types of litter: met, metabolic litter; str, structural litter; wod, woody litter.

BGD
10, 7299–7366, 2013

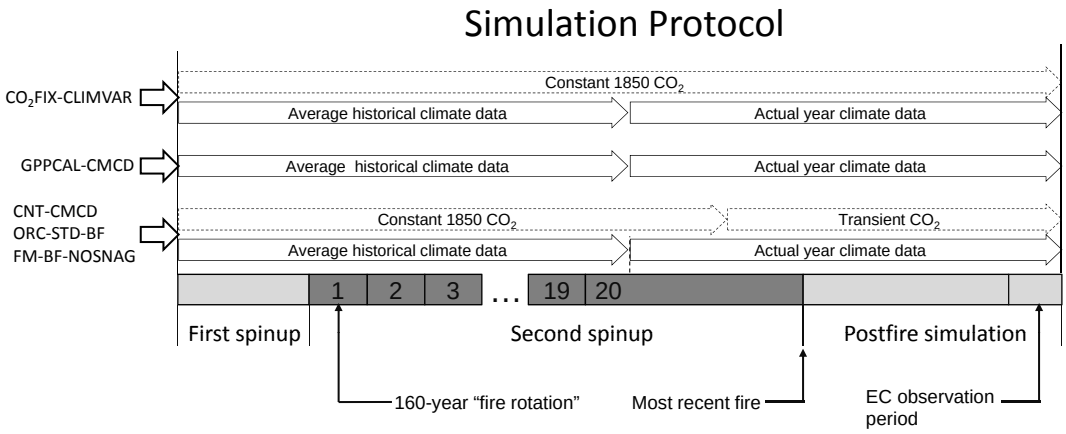

Fig. 3. Illustration of the simulation protocol, climate forcing and atmospheric CO_2 forcing data for various simulations. First spinup: the model is first run for 400 yr starting from bare soil without fire; Second spinup: after first spinup, the model is run for 3200 yr which consists of 20 successive "fire rotations" with assumed crown fires occurring every 160 yr (i.e. a FRI of 160 yr). Postfire simulation: the most recent fire event is simulated during the occurrence year, and the model is driven with actual observed climate forcing data for postfire regrowth. For clarity, CNT-HHCD, GPPCAL-HHCD and CO_2FIX-CLIMFIX simulations were not shown. Refer to Sect. 2.4.4 and Table 4 for more detailed description of different simulations.

BGD
10, 7299–7366, 2013

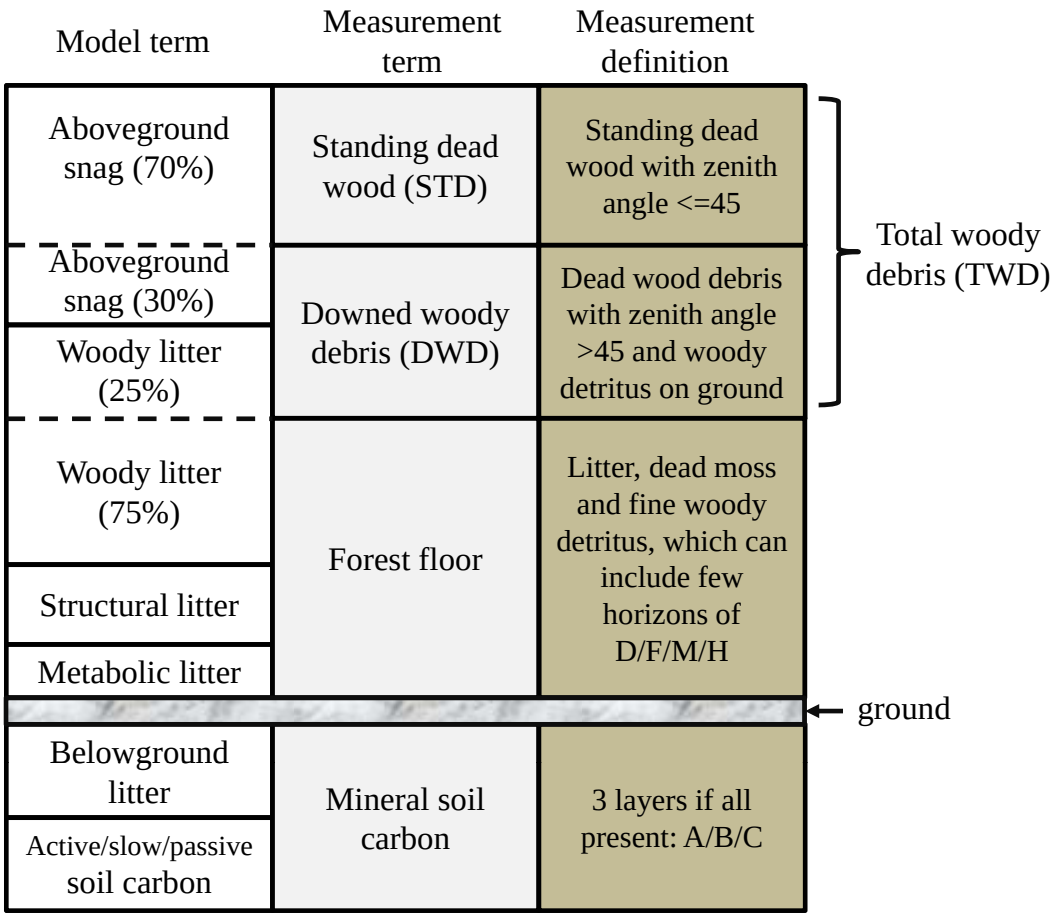

Fig. 4. The scheme for matching model output with field measurements for woody debris, forest floor and mineral soil carbon.

BGD
10, 7299–7366, 2013

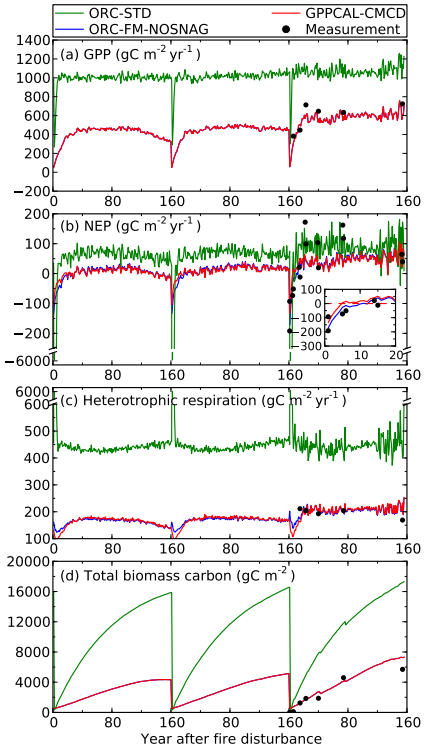

Fig. 5. Simulated **(a)** GPP, **(b)** NEP, **(c)** heterotrophic respiration and **(d)** total biomass carbon for ORC-STD (green), ORC-FM-NOSNAG (blue) and GPPCAL-CMCD (red) simulations, for Manitoba sites. The results are presented for the mean of the seven evaluation sites (CA-NS1 to CA-NS7). The 19th and 20th fire rotation in the second spinup and the postfire simulation after the most recent fire event are shown, with each steep drop of the biomass carbon in subplot **(d)** indicating a fire event. The inset plot within subplot **(b)** shows more details of NEP trajectory for 20 yr after the most recent fire event for ORC-FM-NOSNAG and GPPCAL-CMCD simulations. In subplots **(a)** and **(d)**, blue and red lines overlap with each other.

BGD
10, 7299–7366, 2013

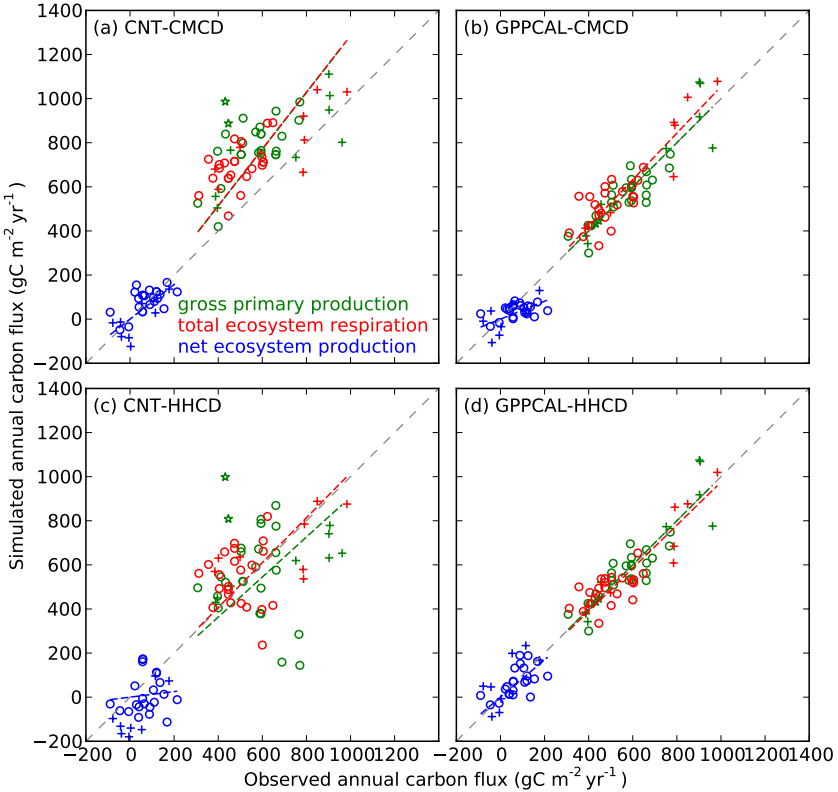

Fig. 6. Simulated versus observed annual gross primary production (green), total ecosystem respiration (red) and net ecosystem production (blue), before (**a** and **c**) and after (**b** and **d**) nudging observed mean multi-year GPP. Observed annual carbon fluxes are from Amiro et al. (2010). 1 : 1 ratio line is shown as the dashed grey line. Colored dashed lines indicate RTO regression lines. Distinctions are made among Manitoba (circles), Saskatchewan (cross symbol, "+") and Alaska (stars) data.

BGD
10, 7299–7366, 2013

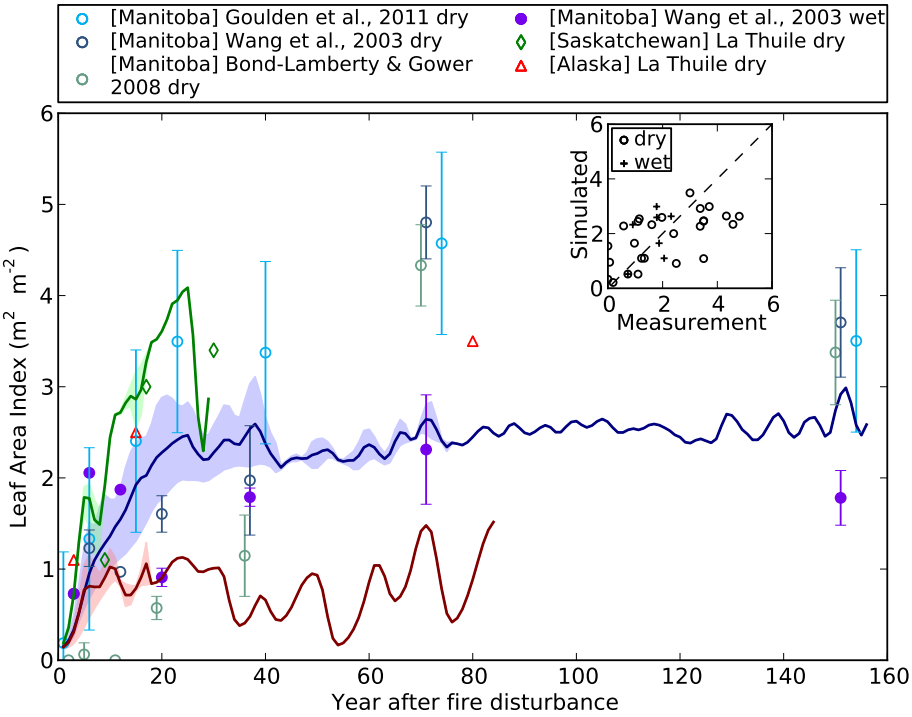

Fig. 7. Simulated and measured leaf area index (LAI) as a function of time after fire. Model results (Manitoba: blue, Saskatchewan: green, Alaska: red) are presented by pooling together outputs for all evaluation sites of the same cluster, with the solid line indicating the mean value, and shaded area showing between-site minimum-maximum range. Measurements from different sources are shown separately for Manitoba (circles), Saskatchewan (diamonds) and Alaska (triangles), with wet (dry) site measurements as filled (open) sign. Error bars on the measurement points indicate 90 % confidence interval measurement uncertainty. The inset panel shows the overall model-measurement agreement along a 1 : 1 ratio line for dry (small open circles) and wet (small cross symbol, "+") site measurements separately.

BGD
10, 7299–7366, 2013

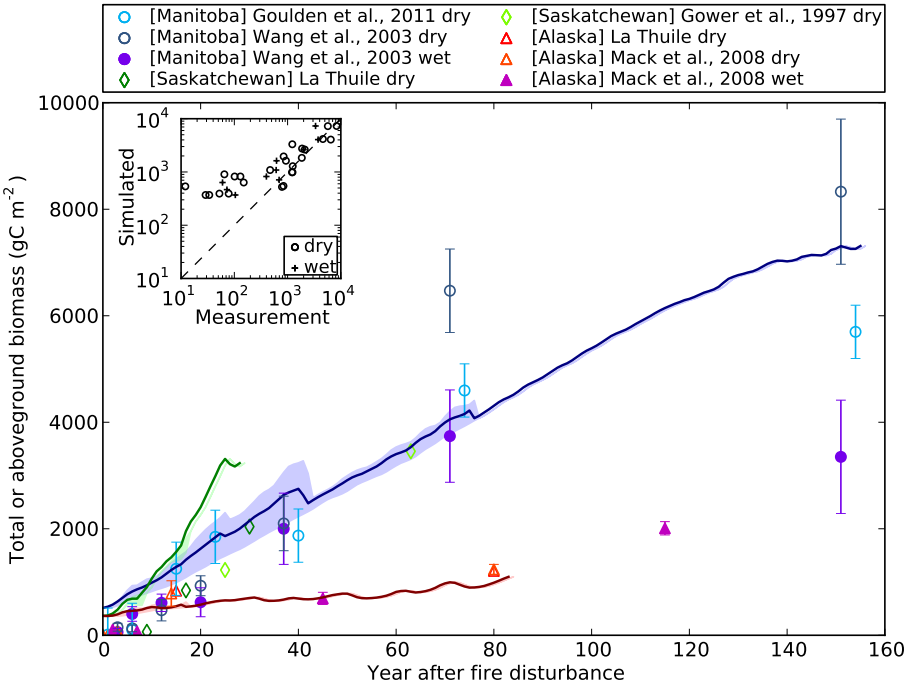

Fig. 8. Simulated versus observed total biomass carbon (for Manitoba) and aboveground biomass carbon (for Saskatchewan and Alaska) as a function of time after fire. Model results (Manitoba: blue, Saskatchewan: green, Alaska: red) are presented by pooling together outputs for all evaluation sites of the same cluster, with the solid line indicating the mean value, and shaded area showing between-site minimum-maximum range. Measurements from different sources are shown separately for Manitoba (circles), Saskatchewan (diamonds) and Alaska (triangles), with wet (dry) site measurements as filled (open) sign. Error bars on the measurement points indicate 90 % confidence interval measurement uncertainty. The inset panel shows the overall model-measurement agreement along a 1 : 1 ratio line for dry (small open circles) and wet (small cross symbol, "+") site measurements separately.

BGD
10, 7299–7366, 2013

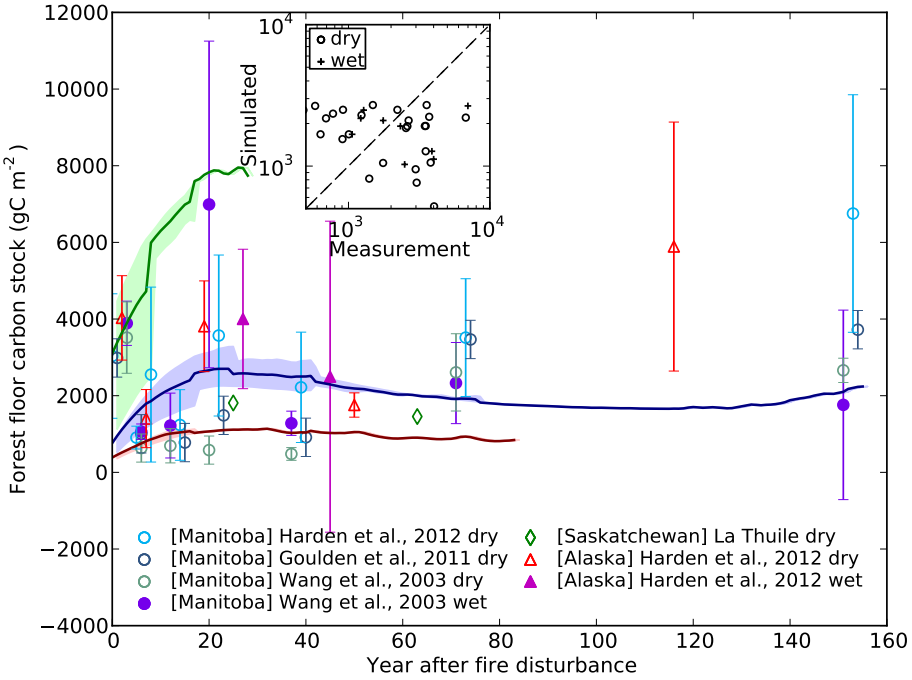

Fig. 9. Simulated versus observed forest floor carbon stock as a function of time after fire. Model results (Manitoba: blue, Saskatchewan: green, Alaska: red) are presented by pooling together outputs for all evaluation sites of the same cluster, with the solid line indicating the mean value, and shaded area showing between-site minimum-maximum range. Measurements from different sources are shown separately for Manitoba (circles), Saskatchewan (diamonds) and Alaska (triangles), with wet (dry) site measurements as filled (open) sign. Error bars on the measurement points indicate 90 % confidence interval measurement uncertainty. The inset panel shows the overall model-measurement agreement along a 1 : 1 ratio line for dry (small open circles) and wet (small cross symbol, "+") site measurements separately.

BGD
10, 7299–7366, 2013

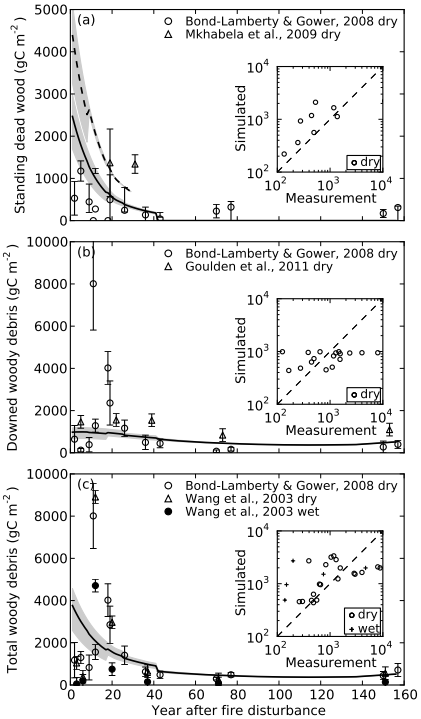

Fig. 10. Simulated versus observed woody debris as a function of time after fire for **(a)** Standing dead wood (SDW); **(b)** downed woody debris (DWD); and **(c)** total woody debris (TWD). Data for Manitoba and Saskatchewan sites are shown for SDW, and only Manitoba sites are shown for DWD and TWD. Model results are presented by pooling together outputs for all the evaluation sites in the same site cluster, with the thick black (and dashed) line indicating the mean value, and shaded area showing between-site minimum-maximum range. All black lines in the three panels show the result for Manitoba sites, the dashed line in panel **(a)** shows the result for Saskatchewan sites. Measurements from different sources are shown for both dry (open circles and triangles) and wet (filled dots) measurements. Error bars on the measurement points indicate 90 % confidence interval measurement uncertainty. The inset panel shows the overall model-measurement agreement along a 1 : 1 ratio line for dry (small open circles) and wet (small cross symbol, "+") measurements separately.

BGD
10, 7299–7366, 2013

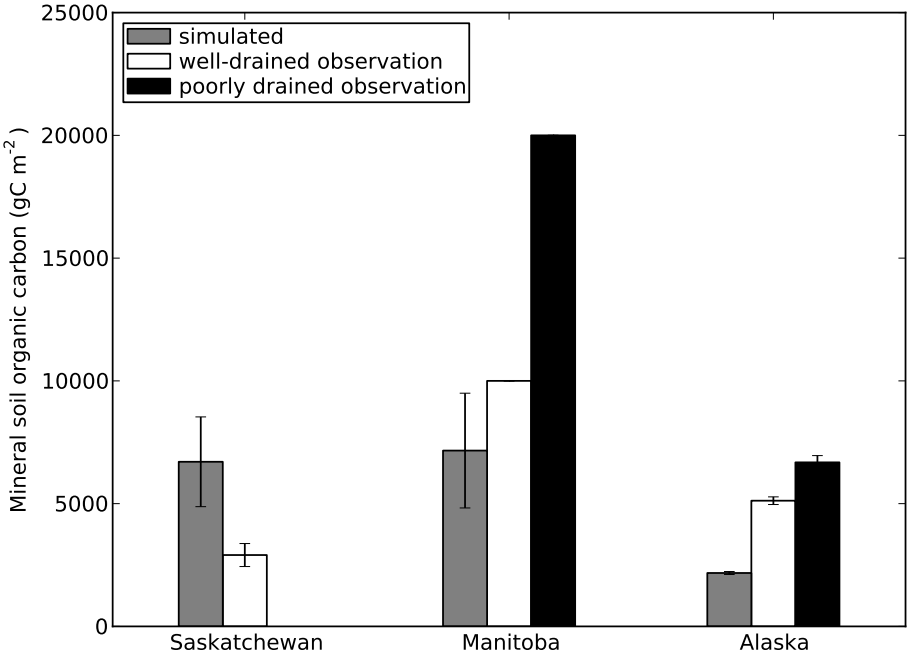

Fig. 11. Comparison of simulated (grey bar) and measured mineral soil carbon (white bar for well-drained observation, black bar for poorly drained observation). Error bars indicate standard deviation among evaluation sites in the same cluster.

BGD
10, 7299–7366, 2013

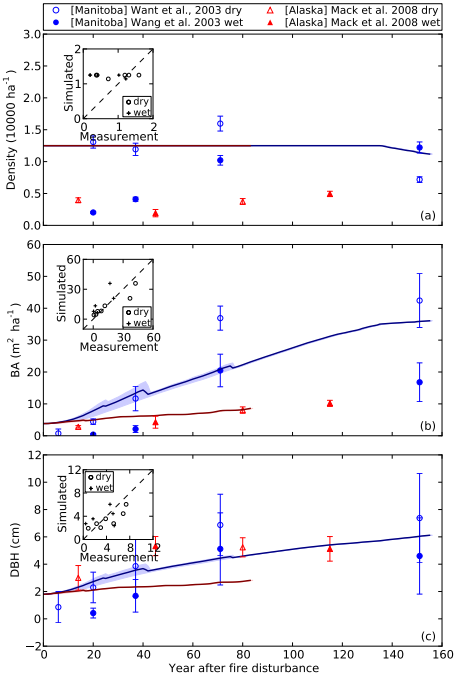

Fig. 12. Simulated versus measured forest **(a)** individual density, **(b)** basal area (BA), and **(c)** mean diameter at breast height (DBH) as a function of time after fire. Observations were only available for Manitoba and Alaska. Model results (Manitoba: blue, Alaska: red) are presented by pooling together outputs for all evaluation sites of the same site cluster, with the solid line indicating the mean value, and shaded area showing between-site minimum-maximum range. Measurements from different sources are shown separately for Manitoba (circles) and Alaska (triangles), with wet (dry) site measurements as filled (open) sign. Error bars on the measurement points indicate 90 % confidence interval measurement uncertainty. The inset panel shows the overall model-measurement agreement along a 1 : 1 ratio line for dry (small open circles) and wet (small cross symbol, "+") measurements separately.

BGD
10, 7299–7366, 2013

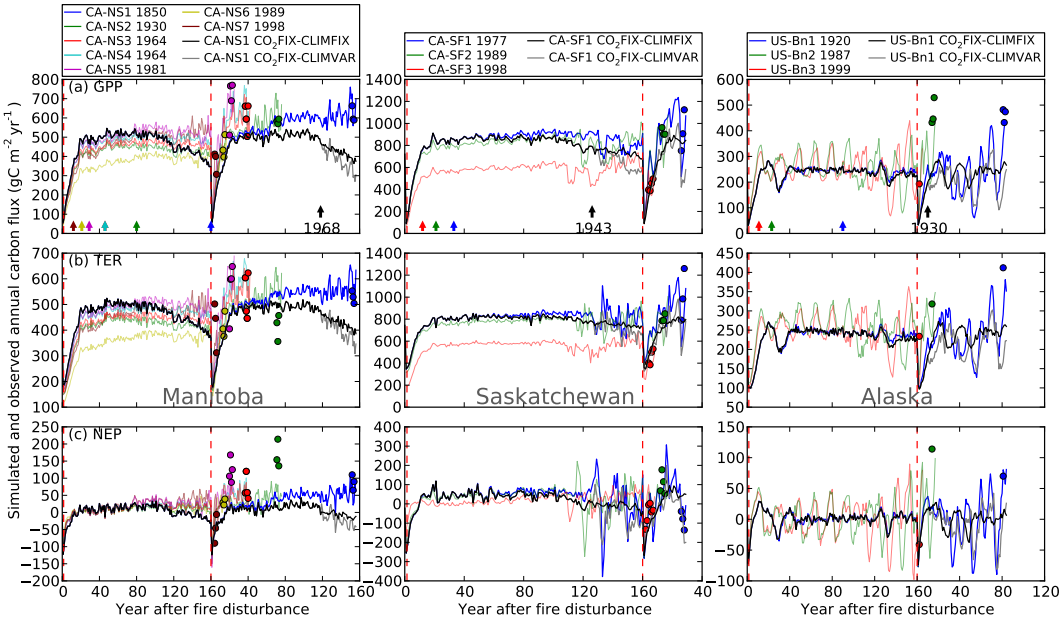

Fig. 13. Simulated GPP **(a)**, TER **(b)** and NEP **(c)** trajectory for the time of the 20th fire rotation (since the first red dashed line) and for the chronosequence period (since the second red dashed line). Simulation results for the scenario of varying CO_2 with varying climate (GPPCAL-CMCD, colored lines) are shown for all evaluation sites in Manitoba (CA-NS1 to CA-NS7, left column), Saskatchewan (CA-SF1 to CA-SF3, middle column) and Alaska (US-Bn1 to US-Bn3, right column). Simulation results for the scenarios of fixed CO_2 with varying climate (CO_2FIX-CLIMVA, grey lines), and fixed CO_2 with fixed climate (CO_2FIX-CLIMFIX, black lines) are shown for the three sites of CA-SF1, CA-NS1 and US-Bn1. Corresponding eddy-covariance CO_2 flux measurements (Amiro et al., 2010; Goulden et al., 2011) at each site were shown as colored dots, with the colors corresponding to the colors of GPPCAL-simulation results for each site. Vertical red dashed lines indicate occurrence of fires. For GPPCAL-CMCD simulation results, the numbers after the site names in the legend indicate the year of most recent fire event. The colored small arrows at the bottom of the first row of panels indicate the time to begin to increase atmospheric CO_2 for each site in the GPPCAL-CMCD simulation, with the color scheme corresponding to the lines in the figure legend. The small black arrows with the numbers indicate the year on each site cluster when the meteorological station observed climate data were available.

BGD
10, 7299–7366, 2013